ACS APPLIED NANO MATERIALS

www.acsanm.org Review

Two-Dimensional Nanomaterials for Moisture-Electric Generators: A Review

Ziheng Feng, Guangyu Hu, Renbo Zhu, Shuo Zhang, Chao Liu, Peiyuan Guan, Mengyao Li, Tao Wan,* Haolan Xu, and Dewei Chu

Cite This: https://doi.org/10.1021/acsanm.2c01557 Read Online

ACCESS | Metrics & More | Article Recommendations

ABSTRACT: As an emerging candidate for a sustainable power supply, moisture-electric generators (MEGs) have attracted great attention in recent years. Unlike the conventional hydroelectric system, MEGs propose to harvest energy from ambient moisture, driven by either ion diffusion under a concentration gradient or the interaction between a solid−liquid interface governed by electrostatic theory. Two-dimensional (2D) nanomaterials, in particular hydrophilic graphene oxide (GO), have been considered as the most promising materials for high-performance MEGs owing to their unique structure and properties. In line with the development of 2D nanomaterials, the recent electrical output of a single MEG has been greatly raised from tens to hundreds of millivolts, which is capable of powering commercial electronics. Herein, we have reviewed the recent progress of 2D nanomaterials in MEGs. The mechanism of moisture-induced electricity generation and strategies for tailoring 2D nanomaterials to enhance the output performance of MEGs are discussed. The potential application of MEGs is also discussed in two categories: sensing and power supply. Finally, the existing challenges and the perspective of MEGs are proposed for future study.

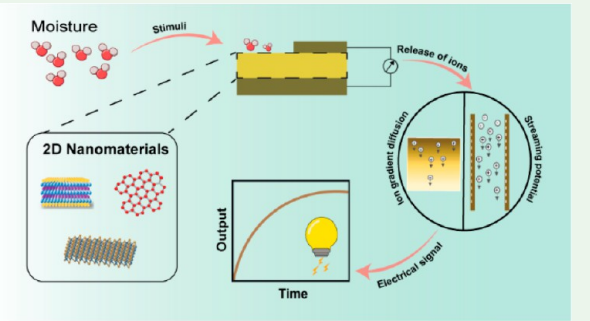

KEYWORDS: *two-dimensional nanomaterials, moisture-electric generator, energy conversion, ion diffusion, streaming potential*

1. INTRODUCTION

The current energy crisis has caught the attention of many of us, especially because most of the existing energy sources (e.g., fossil fuels) produce irreversible pollution to the environment when used, making clean and renewable energy a focal point for the sustainable development of society. In this regard, tremendous work has been done on generating electricity through the conversion of natural sources such as sunlight,[1−3] wind,[4,5] and water.[6−8] Unlike sunlight and wind, which have a periodic output of energy (e.g., sunrise and sunset), water-based electricity such as that from a hydroelectric plant shows a more durational output in electricity generation. However, the hydroelectricity station is strongly reliant on the motion of water flow that converts the mechanical energy into electricity, which somehow restricts its scalable application across fields. And more importantly, the construction of hydroelectric facilities has significant negative impacts on the local aquatic environment.[9] Therefore, the alternative design of a water energy harvester is an emerging topic to be investigated.

In 2006, Wang and Song first proposed the piezoelectric nanogenerator on the basis of a solid−solid surface interaction,[10] opening a trend in developing electric nanogenerators, which benefit the studies of energy conversion from water. When considering water-induced nanogenerators, recent advances focus on converting the energy from the interaction between materials and the diverse forms of water molecules, such as droplets,[11] flows,[12,13] waves,[14,15] and evaporation.[16−18] Very recently, a novel energy harvester called a moisture-electric generator (MEG) has been proposed, inspired by the liquid−solid interaction, which also induces electricity from the ambient environment. Unlike the existing process, the MEG harnesses chemical energy from moisture and converts the energy into electricity. Meanwhile, gaseous water molecules are born with a higher energy state than that of the liquid phase as energy is absorbed during the phase transformation from liquid to gas, making the study of the MEG significantly attractive.[19] The green conversion process is driven by the interaction between the active materials and the ambient moisture. Hence, the selection of materials becomes crucial, in particular, hydrophilic materials that can facilitate

Special Issue: Forum Focused on Australian Authors

Received: April 11, 2022
Accepted: June 22, 2022

the interaction with water molecules are preferable for electricity generation.

After the successful exfoliation of graphene by Novoselov et al., the family of two-dimensional (2D) nanomaterials has flourished in the recent decade.[20] Two-dimensional nanomaterials are characterized by a sheetlike structure with lateral dimensions ranging from nanometers to micrometers, while their thickness varies from one atomic layer to several atomic layers. The current research activity can be found across graphene and its derivatives,[21−23] transition metal dichalcogenides (TMDCs),[24−26] hexagonal boron nitrides,[27−29] transition metal oxides,[30,31] etc. Because of their unique structure and properties, 2D nanomaterials have been widely adopted in applications of energy conversion,[32−34] energy storage,[34,35] optoelectronics,[36] and healthcare.[37,38] In terms of energy conversion, one-dimensional (1D) nanomaterials such as carbon nanotubes (CNTs) have also been utilized to harvest energy from water since 2001.[39] Despite this, 2D nanomaterials [e.g., graphene oxide (GO)] feature a more promising functionality for developing MEGs. On one hand, the existence of a series of functional groups (e.g., hydroxyl, carboxyl, etc.) endows GO with substantial hydrophilicity for absorbing water molecules. On the other hand, the functional groups can be either removed or added through post-treatments. That means the functionality of 2D nanomaterials can be tailored to meet the diverse demands of the MEGs. As to the three-dimensional (3D) nanomaterials such as metal oxide particles, the high internal resistance resulting from the wide band gap can potentially limit the current output.[40] Likewise, as another popular bulk material, polymers generally require a layer of hundreds of micromillimeters to realize a substantial output, certainly enlarging the generator size.[41,42] More importantly, the high surface area of 2D nanomaterials facilitates interaction between water molecules and the materials, thus enhancing the performance of the devices in producing electricity.

In this sense, 2D nanomaterials are more preferable as a demonstrator to illustrate hydrovoltaic performance.[11,12,14] In particular, graphene quantum dots (GQD),[43] GO fibers,[44] GO film,[45,46] and GO foam[47−50] were extensively reported as potential candidates in fulfilling the emerging advances of MEGs. Therefore, it is interesting to propose a systematic work on the evaluation of 2D nanomaterials in MEGs. In this review, first, we will introduce the basic mechanism of moisture-induced electricity generation, followed by a discussion of the current progress of 2D nanomaterials for MEGs. After examining the effect of architecture in MEGs, the potential applications of MEGs are also reviewed (Scheme 1). Furthermore, current issues associated with the development of MEGs are commented on and potential solutions for performance improvement are evaluated accordingly. As a part of the conclusion, prospects are also proposed for the future work in this field.

2. WORKING PRINCIPLE OF 2D NANOMATERIALS IN MEGS

2.1. Concentration Gradient Diffusion. Figure 1 depicts the prevailing mechanism of MEGs associated with 2D nanomaterials.[51] Materials with hydrophilic oxygen-rich functional groups (e.g., −COOH and −OH) have great affinity for water absorption.[52,53] The absorbed water molecules weaken the functional groups, triggering the ionization process, which decompose into mobile positively charged ions (e.g., H^+ ions) and negatively charged groups (e.g., $-COO^-$) due to the solvation effect. The latter are generally stationary and bound to the functional groups' skeleton.[51] With the Grotthuss process, H^+ ions are transported directionally from the side of high concentration to the side of low concentration as the water molecules move, resulting in charge separation and potential generation.[54,55] Fulfilment of the electrical output [e.g., open-circuit voltage (V_{oc})] is indicated when the transportation of mobile ions across the concentration gradient occurs. Meanwhile, a counterbalancing electric field is produced to keep the system in a steady state, whose capacity determines the device output's permanence. Conversely, the electric field will collapse due to the decreasing density of the produced protons, revealing the decay of the electrical signal. That says that the mobile ions migrate back toward the counter immobile ions group for recombination. As a result, until the next cycle of moisture input, the energy production will progressively drop to a null state.

Herein, an establishment of the ion concentration gradient within the moisture-harvesting layer is crucial for electricity generation. In general, the ion concentration gradient can be generated by realizing an asymmetric intake of moisture within the functional groups. In this regard, a high concentration of charged ions is formed at the side with high moisture input, whereas a low concentration of charged ions is formed on the other side that encounters a low moisture input. Likewise, a water-proof layer is also applicable on one side of the functional layer to prevent the entry of moisture. The region exposed to ambient moisture will first generate a dense concentration of mobile ions. Conversely, a low concentration of mobile ions is formed at the covered side. On the other hand, post-treatments such as moisture-electric annealing (MeA),[46] selective laser irradiation,[47,56,57] thermal annealing,[48] and UV oxidation[45] are also extensively applied to the pristine samples for constructing the asymmetric content of oxygen functional groups.

Scheme 1. Schematic Illustration of Moisture-Electric Generators: 2D Nanomaterials, Mechanism, Architecture, and Applications

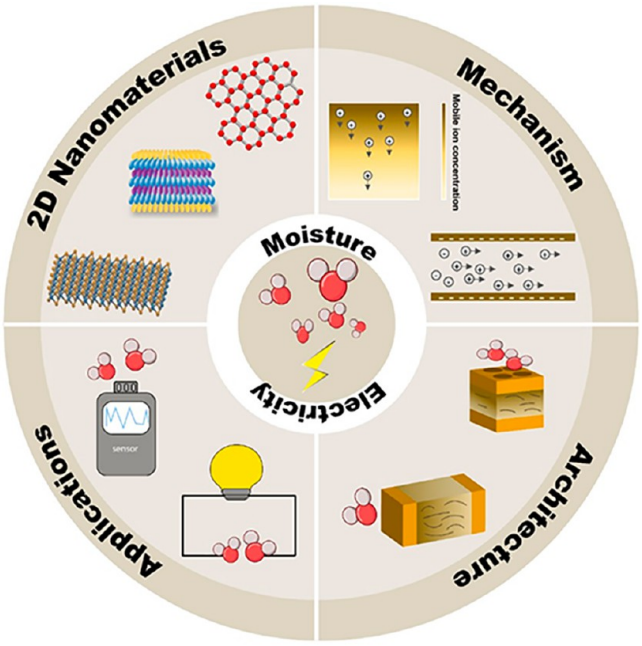

https://doi.org/10.1021/acsanm.2c01557
ACS Appl. Nano Mater. XXXX, XXX, XXX−XXX

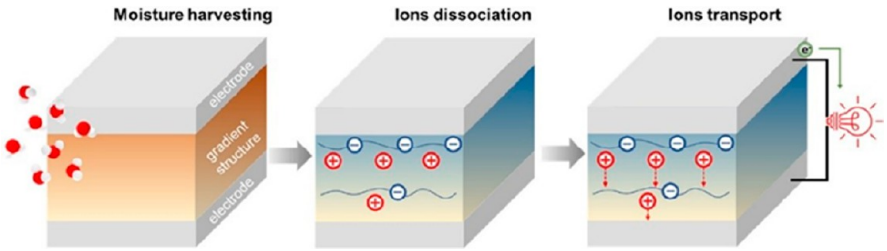

Figure 1. Mechanism of generating electricity upon moisture exposure based on an ion concentration gradient. Reprinted with permission from ref 51. Copyright 2021 American Chemical Society.

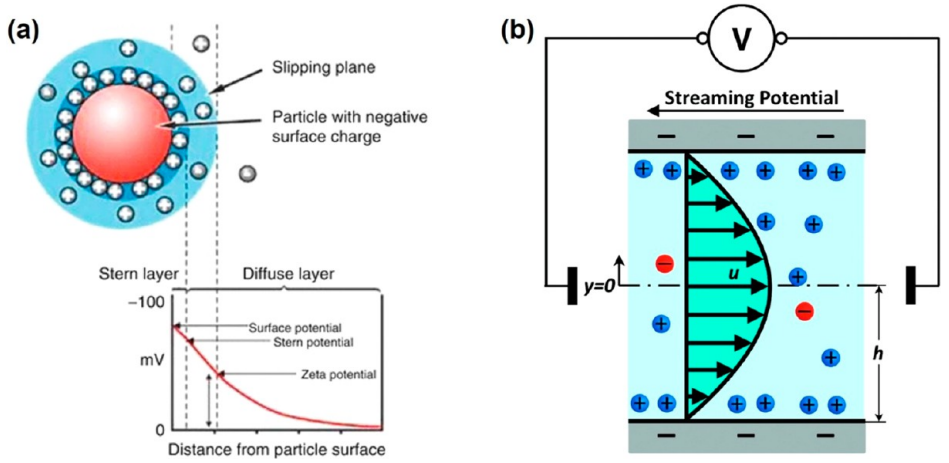

Figure 2. (a) Scheme of the electrical double layer. Reprinted with permission from ref 58. Copyright 2016 Springer Nature. (b) Schematic illustration of the streaming potential. Reprinted with permission from ref 62. Copyright 2018 Royal Society of Chemistry.

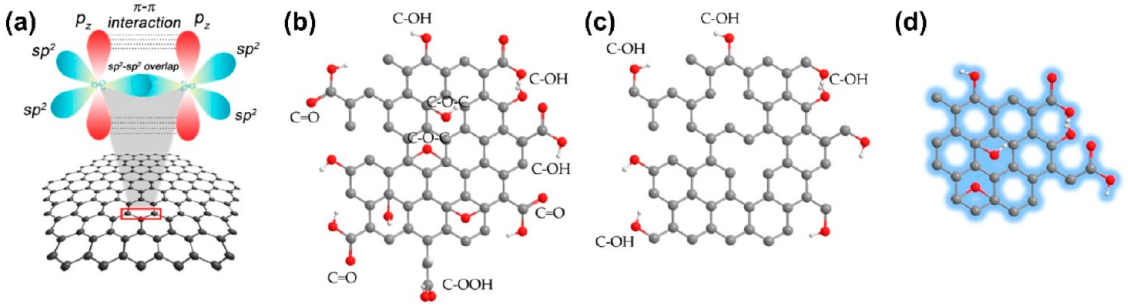

Figure 3. Scheme of (a) graphene, (b) graphene oxide, (c) reduced graphene oxide, and (d) graphene-based quantum dots. Reprinted with permission from ref 68. Copyright 2017 MDPI.

2.2. Streaming Potential. Harvesting energy from water based on a liquid−solid interaction can be traced back thousands of years. With the growth of scientific research, more insights are put into the microstructure instead of the macrostructure. In the 1800s, Quincke found that electricity was induced by a fluid flow within small channels, with the aid of the capillary effect. The phenomenon of electricity generation from the interaction between a liquid and solid surface is dominated by the streaming potential, governed by electrokinetic theory. To illustrate the mechanism, the electrical double layer (EDL) is an essential model. In general, the EDL is composed of two layers with a thickness measured as the Debye length, one of which is an inner layer that possesses a charged solid surface. Owing to the electrical attraction effect, the counter ions regarding the solid surface charge are firmly attracted to form a layer called a stationary Stern layer. In contrast, a cloud of mobile ions originating from the inflow liquid is present in the outer layer called the diffuse layer (Figure 2a).[58] Note that an interface exists distinct to the layer of either the stationary or mobile part where a water−liquid interaction starts to occur, which is called the slipping plane, with an intrinsic potential (ζ-potential). The potential indicates the surface charge of the particle and the reactivity between particles in the suspension.[59] As shown in Figure 2b, when water molecules flow through a channel where the EDL of two surfaces overlaps, counter ions are highly mobile under the attraction of the oppositely charged solid surface, enabling ion migration under a pressure gradient.[60−62] Conversely, ions with the same polarity as the surface charge are confined and accumulate at the location. Consequently, the separation of ions induces a potential called the streaming potential.

Under the framework of the streaming potential, the ζ-potential regulates the contact between the solid and liquid interfaces. Theoretically, a strong repulsive force between solid particles exists in the dispersion when the particles are of high ζ-potential. Flocculation of particles is avoided, and particles

https://doi.org/10.1021/acsanm.2c01557
ACS Appl. Nano Mater. XXXX, XXX, XXX−XXX

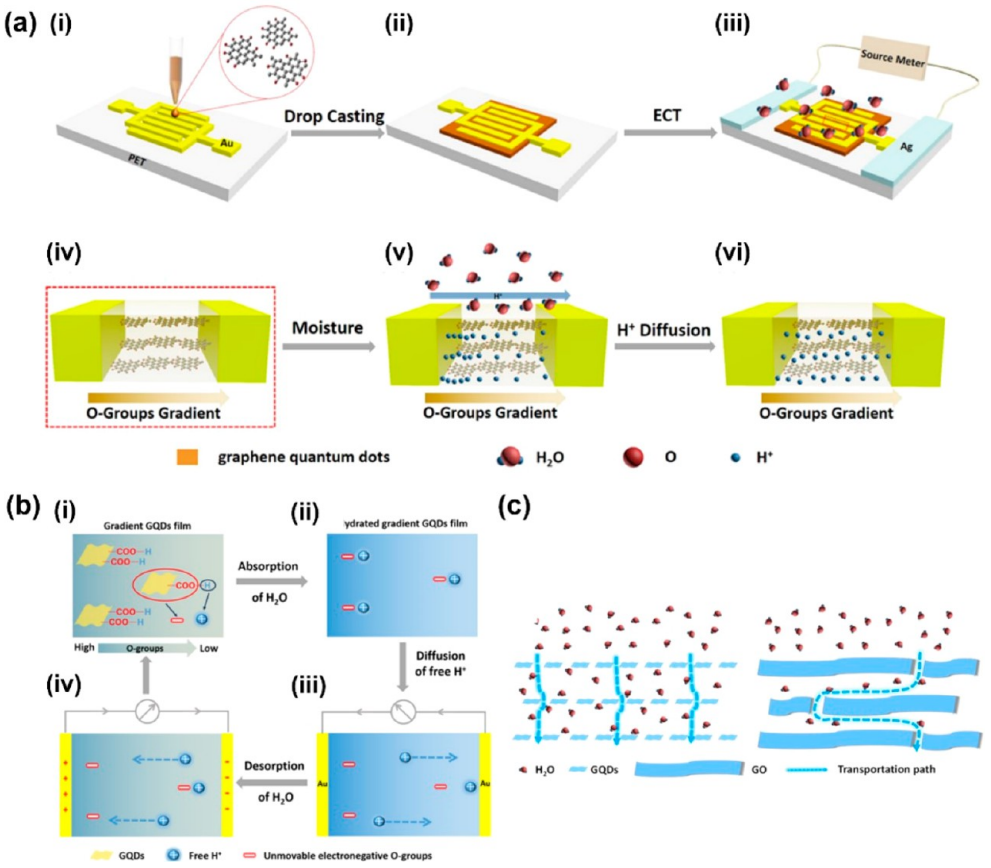

Figure 4. (a) Schematic illustration of the GQDs-based MEG. (b) Mechanism of the generation of electricity when water molecules are absorbed by GQDs film. (c) Pathway for ion migration in GQDs film (left) and GO film (right). Reprinted with permission from ref 43. Copyright 2017 American Chemical Society.

become active to attract more charges, resulting in enhancing the interaction in the solid−liquid interface. On this aspect, it has been learned that the ζ-potential is impressively influenced by the pH of the working medium, where the alkaline/acidic condition prefers to provide a higher ζ-potential.[60,61,63] Therefore, relative adjustment could be considered when the streaming potential dominates the electricity generation. On the other hand, it is also suggested that the porosity and the diameter of the nanopores are crucial in achieving the ion-selective permeation, which is a prerequisite for a desirable output performance.[61]

3. 2D NANOMATERIALS IN MEGS

3.1. Graphene-Based Materials. In nature, carbon is ubiquitous, and its diverse forms have been widely adopted across many fields. Graphene, which appears as a single layer of graphite in a honeycomb structure, has been utilized as a rising candidate of carbon materials in recent decades (Figure 3a). Each carbon atom within the lattice pairs with the other three neighbors with σ-bonds and an extra bond that is out of the plane, termed a π-bond.[64] From the study of the electron configuration, it was found that the 2p orbital of the carbon atom in the excited state is in charge of the formation of the π-bonds. Thus, the bonds are intrinsically active, which offers a great freedom in tuning the functionality of graphene. The well-known Dirac fermions are a consequence of π-bonds, which endow graphene with a zero band gap and hence an exceptional electrical conductivity.[65] Meanwhile, the out-of-plane location of the π-bonds is an advantage in the interaction with chemical compounds, particularly water molecules for MEGs. Therefore, there is great potential in developing MEGs with graphene-based materials. However, the zero band gap and semimetallic nature of graphene impede its application in semiconducting electronics that require a defined band gap.[66,67] Thus, the promising trend in the study of graphene has shifted to engineer 2D graphene nanosheets into alternating allotropies to overcome the drawbacks (Figure 3).

3.1.1. Graphene Quantum Dots. Graphene quantum dots are the products of etching a single layer of graphene flake, developed after the introduction of graphene in 2008 (Figure 3d). Unlike carbon quantum dots (CDs), GQDs are constructed by confining graphene lattices within a dot with a size of less than 100 nm and no more than 10 layers in thickness.[69] The zero-dimensional structure endows GQDs with unique quantum confinement and a large edge effect, which affects the electron distribution and leads to the modification of the band gap. Additionally, the chemical and physical properties of GQDs are strongly reliant on the composition, size, and shape and can be modified by doping or using different fabrication methods.[70−72] In this regard, the tunable properties of GQDs broaden their potential applications in energy storage and conversion, such as moisture-enabled electricity generation. For example, Huang et al. constructed a highly efficient GQDs-based MEG with quantum dots with a size of 2−5 nm that was capable of generating a voltage and power density of 0.27 V and 1.86 mW/cm^{-2}, respectively.[43] An electrochemical treatment (ECT) process was conducted on the GQDs film to form a

https://doi.org/10.1021/acsanm.2c01557
ACS Appl. Nano Mater. XXXX, XXX, XXX−XXX

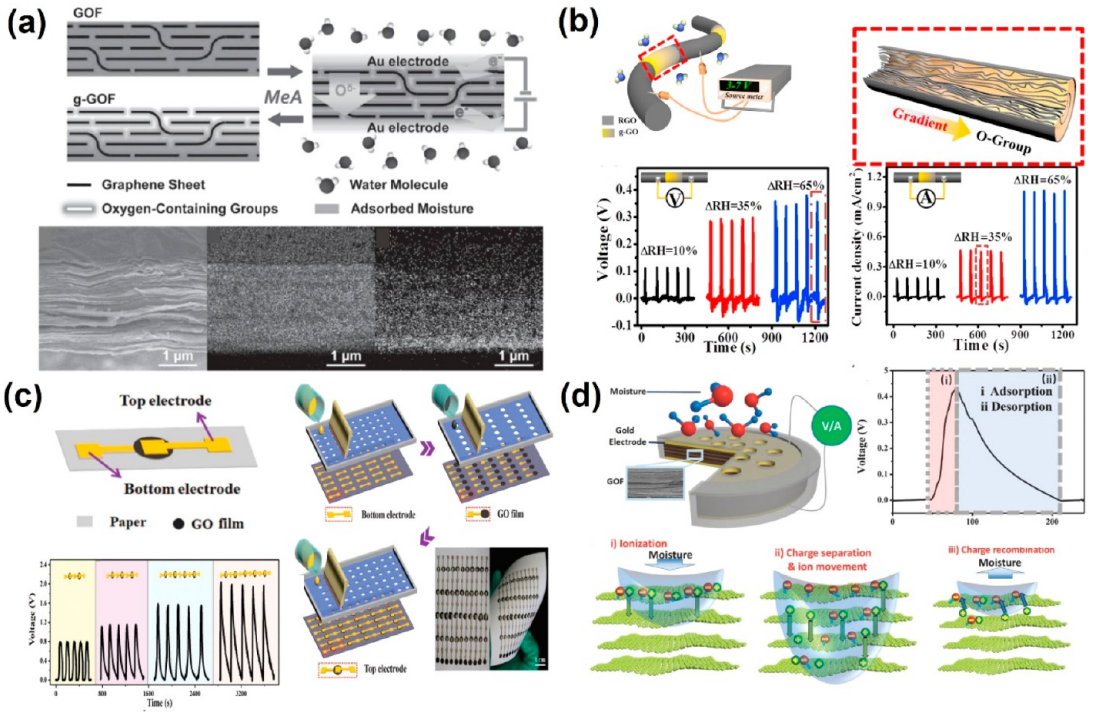

Figure 5. (a) MeA process for the preparation of a gradient GOF. The scanning electron microscopy (SEM) image shows the lamellar structure of the GOF in cross section. Examination of the oxygen mapping within the GOF (left) and gradient GOF (right) through energy-dispersive X-Ray analysis (EDX). Reprinted with permission from ref 46. Copyright 2015 Wiley-VCH. (b) Electricity generation from the 1D GO fiber. Reprinted with permission from ref 75. Copyright 2017 Elsevier. (c) The screen-printed flexible GO-based MEG. The output performance could be significantly improved by printing in serial. Reprinted with permission from ref 77. Copyright 2018 Royal Society of Chemistry. (d) The pristine GO is sandwiched between two pieces of Au electrodes, where the top electrode has holes for moisture intake. A large number of protons are ionized within the GO near the top electrode, which diffuse toward the bottom where water is impenetrable due to the solid bottom electrode. Reprinted with permission from ref 55. Copyright 2018 Wiley-VCH.

gradient of oxygen-containing functional groups by applying a constant bias voltage. Because of the ion gradient diffusion, mobile H^+ ions are dissociated from the functional groups when the water molecules are absorbed (as shown in Figure 4, parts a and b).

Furthermore, the microstructural observations indicated the existence of abundant defects within the GQDs, such as edges and active sites, which offer more oxygen-containing functional groups to enhance the interaction between the absorbed water molecules and the active species. The zero-dimensional configuration of the GQDs also endows the device with the advantage of proton migration. As shown in Figure 4c, the novel structure of the GQDs film enables a short transportation distance of moisture and thus avoids the plugging of water molecules during transportation, which was a concern with the lamellar materials. Taking all this into account, a substantial electrical output is achieved with the GQDs-based device.

3.1.2. Graphene-Based Films and Fibers. The former proposal has demonstrated the importance of the presence of oxygen functional groups in the graphene-based MEGs. Even though 2D graphene shows exceptional electrical performance in terms of a large carrier mobility (200 000 cm^{-2} V^{-1} s^{-1}) and electrical conductivity (6.6 MS m^{-1}), it could not be directly applied in MEGs before manually introducing oxygen-containing groups.[73] In this manner, there is a significant advantage of GO over the pristine graphene. By the virtue of the activity of the π-bonds, graphene can be easily manipulated chemically to endow it with various functionalities.[53,65,74]

In 2015, Zhao et al. first proposed a power generator through harvesting energy from moisture based on a GO film (GOF).[46] To fulfill the requirement of constructing the ion concentration gradient, the GOF was processed through MeA to build up a gradual content of oxygen-containing groups, where oxygen-containing groups are rich on one side and the other side has little of the groups (as shown in Figure 5a).[46] When the gradient GOF was exposed to moisture, a larger number of protons were released from the side rich with oxygen-containing groups than the other side. In this regard, the gradient of protons is formed that triggers the movement of ions from the rich side to the poor side.

Beyond the 2D film structure, Qu's team integrated a nanogenerator with a textile by developing 1D sandwich-like reduced GO (rGO)/GO/rGO fibers, which offer a larger active surface area than the 2D film.[75] As shown in Figure 5b, stacked layers of GO are compacted and aligned to construct the fiber. Subsequently, the pristine GO fiber is selectively laser-irradiated to remove the oxygen-containing groups to obtain the alternating rGO/GO/rGO structure.[76] GO, located in between the adjacent rGO, is processed through MeA to generate a gradient of the functional groups. The reported 1D fiber could be bent at 80° for 1000 cycles without significant degradation in voltage output, showing great potential in self-powered wearable applications. Along with the superior mechanical flexibility, a single GO-based fiber with a diameter of 80 μm and a length of less than 1 mm is capable of generating a voltage of 0.4 V at a relative humidity (RH) of 65%.[75] This advantage of the graphene-based nanofibers can

https://doi.org/10.1021/acsanm.2c01557
ACS Appl. Nano Mater. XXXX, XXX, XXX−XXX

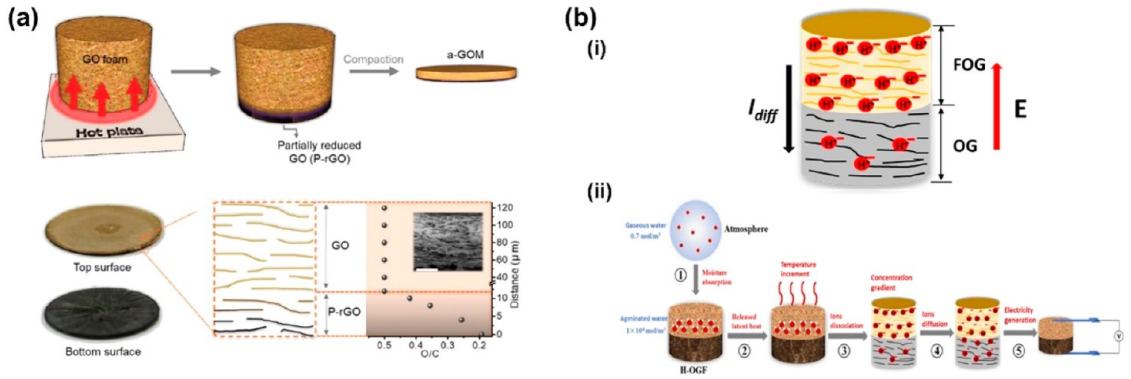

Figure 6. (a) Scheme of the development of rGO on the GO monolith. The thermally annealed region of the bulk GO transforms from brown to dark gray, indicating the partial reduction of GO to rGO. Reprinted with permission from ref 48. Copyright 2018 Royal Society of Chemistry. (b) (i) Schematic illustration of the compacted FOG/OG bulk material. (ii) Proposed initiated mechanism of the MEG. The energy gap between the gaseous and agminated moisture works as the activation energy to trigger the first step of hydrolysis of the oxygen-containing functional groups. Reprinted with permission from ref 78. Copyright 2022 Elsevier.

be even conspicuous when the serial connection is constructed, in which the voltage is proportional to the number of connected devices.

However, the above process is restrained by the complicated post-treatment of the GO. To promote a scalable production for practical application, direct screen printing was introduced to fabricate the GO film-based MEG (as shown in Figure 5c).[77] After the synthesis of the GO solution, the fabrication of an MEG device is accomplished in three steps. A bottom electrode is first screen-printed on a piece of paper. Then, the bottom electrode is overlaid with the as-synthesized GO solution through screen printing, followed by another round of electrode printing on top of the GO-covered side to construct a completed circuit. The facile fabrication process contributes a great potential for realizing the scalable production of flexible MEG devices. It is also easy to manufacture the devices in series/parallel connections for realizing high output performance. Similarly, the pristine GO film was employed as the active material to generate power by Xu's team in 2018.[55] Two pieces of gold film are used as electrodes, one of which is porous for the penetration of moisture (as shown in Figure 5d). It demonstrated a good example of an asymmetric input of moisture in generating electricity. The directional input of water molecules stimulates the generation of mobile ions and the corresponding directional ion migration. Without any treatment, a single coinlike MEG device is capable of generating a transient potential of 0.4−0.7 V upon exposure to an RH of 70%.[55]

3.1.3. Bulk Graphene-Based Materials. Currently, most of the graphene-based MEG devices are subject to the generation of transient output, which is attributed to insufficient mobile ion generation and difficulty in transporting the ion in a unique direction. The transient output is significantly not suitable for an application that requires a stable supply of energy. In contrast to the low-dimensional structure, 3D GO affords a greater specific surface area to atmospheric moisture, making it promising for continuous energy harnessing.

To prove the feasibility, an MEG was fabricated on the basis of a GO foam that was thermally annealed unidirectionally on a hot plate. The reason for annealing is to partially reduce GO to rGO.[48] As shown in Figure 6a, a consistent content of oxygen-containing groups is found in the GO while a gradual decrement of that is present in partially reduced GO (p-rGO). Similar to the reported bulky gradient GO foams as active materials that are treated through the MeA process,[50] the thermally annealed GO/p-rGO possesses an intrinsic gradient of oxygen functional groups. Because of the porous structure of 3D graphene, a great amount of moisture can be absorbed. The proposed device was able to demonstrate a voltage output of up to 450 mV at an RH of 85% that could be sustained for 500 s and could even maintain the output at 180 mV for 100 h at an RH of 16−26%.

Very recently, an approach that combined the advances discussed above in the 3D graphene-based MEG has also been recommended. Unlike the conventional GO-based MEG devices, oxidized graphene (OG), which possesses fewer oxygen-containing functional groups, was employed in this experiment. To construct the ion concentration gradient, the OG powder was fluorinated in order to be anchored with fluorine. The monoliths of fluorinated oxidized graphene (FOG) and OG were compacted through dry-compressing to fabricate the 3D heterogeneous structure denoted as H-OGF.[78] By doing so, the fabricated device has recorded an exceptional output of 1.2 V upon exposure to moisture of 90%, which could even last for more than 40 000 s. In the system, the shortlisting of fluorine (F) becomes the dominant contributor (Figure 6b). First, the introduction of fluorine to graphene triggers the formation of C−F bonds, of which the large polarity enlarges the affinity of the interaction with water molecules. Besides, it is known that the ionization ability is correlated with acidity, where a strong acidity is more favorable under the working principle of MEGs. The high magnitude of the electronegativity endows fluorine with strong acidity, which is also reflected in experimental results. Therefore, fluorine is empowered to attract electrons that can stimulate the ionization of the oxygen-containing functional groups in an extremely active manner. Note that the novel design employed OG instead of GO. Compared to GO, the higher value of pH in OG is more capable of hindering the process of ionization. Combined with the weaker affinity for water absorption of OG compared to FOG, it further enables a greater ion concentration gradient when fabricating the device in coupling with FOG. The second step to realize a comprehensive enhancement in performance is revealed by modification of the morphology. The interplanar distance of OG is significantly broadened when fluorine is present. As such, ion migration is accelerated, allowing the device to have a faster response time.[79,80] Interestingly, the team also proposed a comprehen-

https://doi.org/10.1021/acsanm.2c01557
ACS Appl. Nano Mater. XXXX, XXX, XXX−XXX

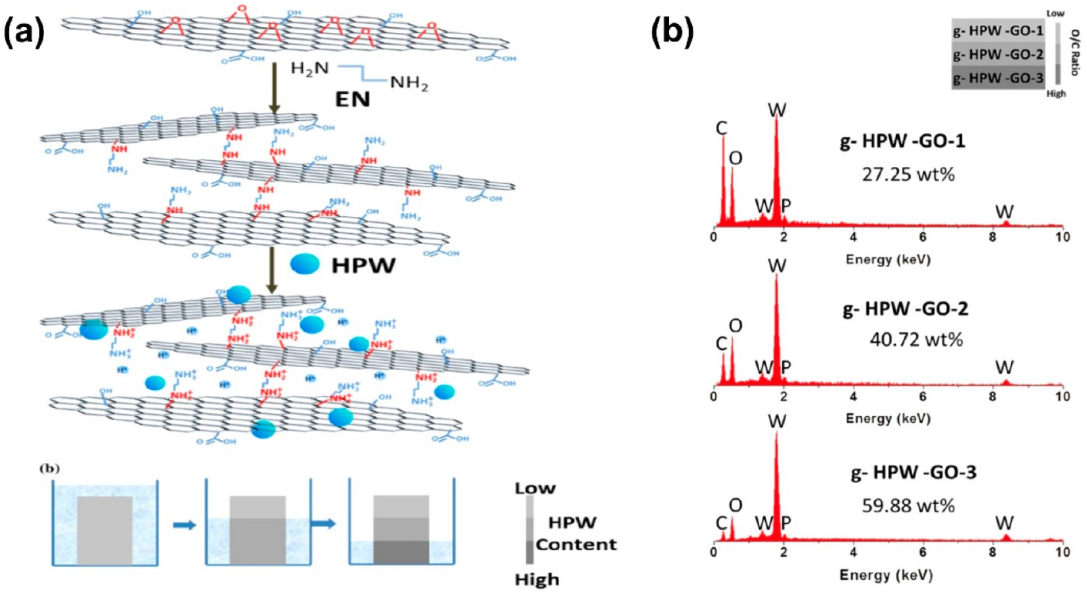

Figure 7. (a) Synthesis of the g-HPW-GO monolith. (b) Energy dispersive X-ray analysis (EDAX) patterns of the g-HPW-GO monolith, indicating the bottom region with the highest content of oxygen-containing groups, since most HPW solution is absorbed by the part. Reprinted with permission from ref 54. Copyright 2018 Springer Nature.

Table 1. Comparison of MEGs Consisting of Graphene-Based Materials with Different Treatments

material	architecture	treatment	electrical output	ref
GQDs	quantum dots	MeA	0.27 V, 1.86 mW/cm^2	43
GO fiber	nanofibers	laser irradiation and MeA	0.35 V, 1.06 mW/cm^2	75
GO	film	MeA	0.035 V, 0.42 μW/cm^2	46
GO	film	no treatment, pristine	0.7 V, 25 μA/cm^2	55
GO	film	element intercalation (K^+ ions)	1.2 V, 2.5 μW/cm^2	84
GO	film	acidification (HCl)	0.85 V, 92.8 μA/cm^2	82
GO	bulk	thermal annealing	0.45 V, 2.02 μW/cm^2	48
OG	bulk	fluorination	0.75 V, 9 μW/cm^2	78
GO	bulk	acidification (HPW)	6.2 μA/cm^2, 0.07 μW/cm^2	54
rGO	composite	rGO/BCP	1.15 μW/cm^2, 6.40 μA/cm^2	90
GO	composite	GO/PAAS	0.2−0.6 V, 0.07 μW/cm^2	49
rGO	composite	SA/SiO_2 nanofibers/rGO	0.5 V, 100 μA (absorption)	93
			0.5 V, 50 μA (desorption)	

sive explanation of the activation energy reserved for the ionization of the functional groups. As mentioned in the earlier section, gaseous moisture is intrinsically high in internal energy.[19] As shown in Figure 6b, part ii, the adsorbed moisture can transfer into the agminated state that possesses lower internal energy. Thus, the energy difference induced by the phase transformation results in latent heat. It can act as the activation energy for the ionization of functional groups to occur.[78]

3.1.4. Modulated Graphene-Based Materials. As mentioned in the earlier section, the Grotthuss mechanism dominates the proton transportation when oxygen-containing functional groups encounter water molecules. A higher RH can introduce a higher content of water molecules, in which more hydrogen-bonding networks are established for hydrolysis to occur. However, to realize the widespread promotion of the devices for daily usage, it is necessary to expand the range of the applicable humidity. Otherwise, work is required to regulate the materials for greater aptitude in interacting with the mobile ions. Liu et al. promoted the performance of a GO-based MEG device.[54] A 3D spongelike GO was immersed into phosphotungstic acid (HPW) and soaked in order to construct a gradient distribution of HPW on GO, as shown in Figure 7, parts a and b. HPW has the virtue of high proton conductivity, which was previously proven.[81] The embedding of HPW becomes an approach to enhance the proton conductivity of GO. In addition, the 3D configuration of GO is in charge of extending the output duration, since the pathway for H^+ diffusion is elongated, and hence H^+ requires a longer time for either discharging or output degradation. An MEG composed of GO/poly(vinyl alcohol) (PVA) was also acidified with HCl to study the effect of the combination of the above treatments on GO.[82] The acidification process can significantly increase the ratio of C═O bonds within the functional groups of GO, boosting the competence in attracting the mobile charge carrier when ionization of the active film occurs under a humid environment.[83] The effect is improved with the concentration of HCl and optimized when 32% HCl is employed. Therefore, the integration of acidification and polymer insertion on GO assists the device to surprisingly achieve a voltage and current density of 0.85 V and 98.2 μA cm^{-2}, respectively, at an RH of 75%.

https://doi.org/10.1021/acsanm.2c01557
ACS Appl. Nano Mater. XXXX, XXX, XXX−XXX

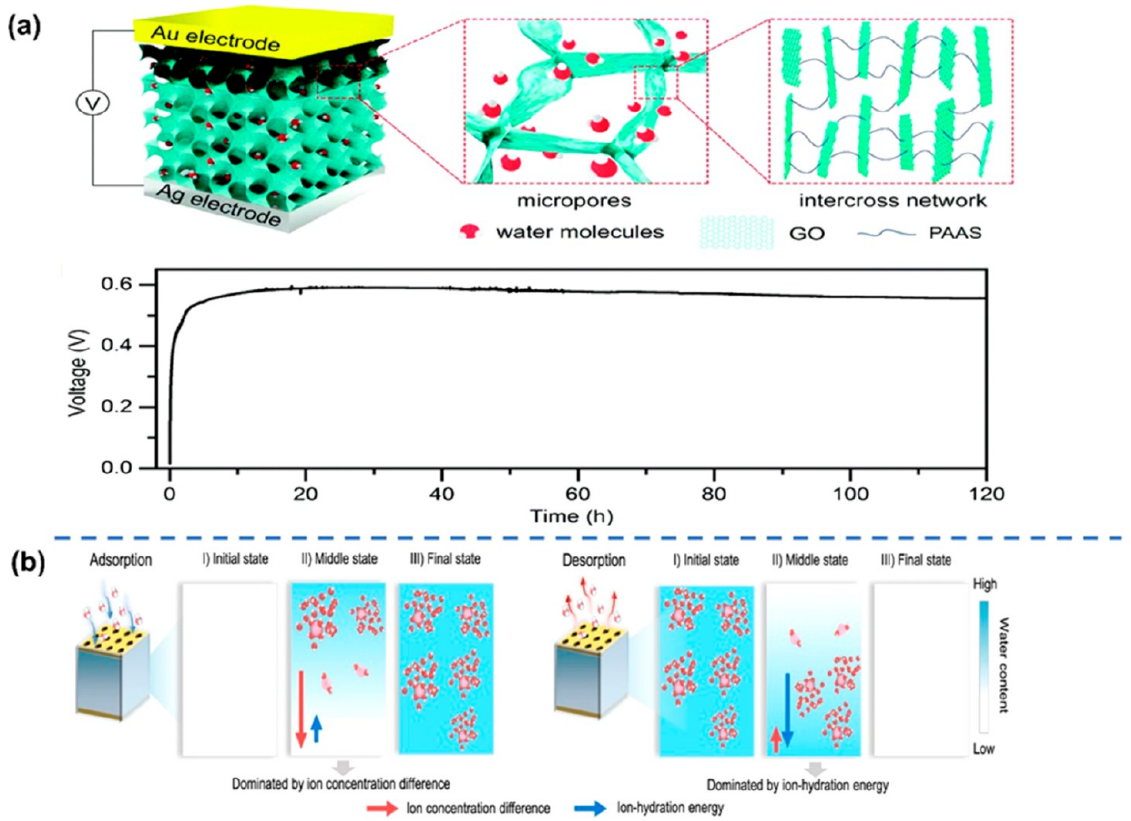

Figure 8. GO composite-based MEGs. (a) Illustration of the composite GO/PAAS MEG. Each GO sheet is connected by the chainlike PAAS, enlarging the hydrophilic surface of the device. Reprinted with permission from ref 49. Copyright 2019 Royal Society of Chemistry. (b) Proposed mechanism for electricity generation subject to water absorption and desorption. Reprinted with permission from ref 93. Copyright 2022 Springer Nature.

Inspired by electric eels, a novel solid-state power source was also developed based on GO ink.[84] In contrast to the aforementioned devices, the reported cell has an extremely superior capability for electricity generation of up to 1.2 V per unit at an RH of 10%. Unlike the previously proposed MEGs, which are powered by the hydrolysis of GO, potassium hydroxide (KOH) solution is mixed with the GO ink for the creation of the ion concentration gradient. The low magnitude of the intrinsic characteristics of potassium (K) ions (e.g., hydrated ionic radius and ionic charge) stimulates its ion transportation in a humid environment, which is favorable for moisture-induced electricity generation.[85] Reaction with the functional groups occurs when KOH is added into the GO solution, leading to the removal of the oxygen functional groups from GO to form rGO. Thus, a higher concentration of K^+ is established in rGO compared to the pristine GO. Because of the negatively charged surface, the interlayer spacing of GO and rGO is open for cation transportation from the rGO side to the GO side upon exposure to ambient conditions. Thus, the potential difference is induced under the migration of cations. Additionally, with aid of the feasible printing technique, a voltage of 192 V is realized by connecting 175 units in series fabricated on a piece of paper, demonstrating scalable production for practical applications. Note that the V_{oc} decreases with the increment of humidity, which can be attributed to the offset of the ion concentration gradient by the hydrolysis of pristine GO within the device, showing an opposite way to that of conventional MEGs but a great potential for application in low-humidity conditions. Table 1 compares the performance of MEGs consisting of graphene-based materials with different treatments.

Additionally, the redox reaction on the coupled electrodes was explored in the study. Gold and silver, respectively, were used as the current collector to study the effect. With the employment of gold, a transient output is detected that is of a similar performance with that of the previously reported MEG devices. Likewise, the ion movement is in charge of both the induced voltage and current in this case via charge adsorption on electrodes. Thus, the charge adsorption in gold electrodes is highly reliant on the surface condition. However, a boost in capacity is realized by replacing gold electrodes with silver. A redox reaction was observed at the silver electrode. In this manner, the generation of voltage and current is triggered in two separate processes. Electric voltage is provided by the ion concentration difference as usual, but the current is induced by the conversion of ion migration to electron transportation through the consecutive redox reaction. Thus, the device can achieve a more stable electrical output than that of the gold electrodes.

3.1.5. Graphene-Based Composite Materials. On the basis of the above proposals, the electrical output performance of GO-based MEGs is directly related to the relative humidity,[86] where a high RH is mostly preferable. Regardless of the substantial proton conductivity of GO, the epoxide group located at the basal plane of GO risks getting deactivated with time.[86] Meanwhile, a challenge arises from the strong intrinsic stacking force of GO, which leads to the aggregation of GO nanosheets. As such, an increment of the internal resistance is

https://doi.org/10.1021/acsanm.2c01557
ACS Appl. Nano Mater. XXXX, XXX, XXX−XXX

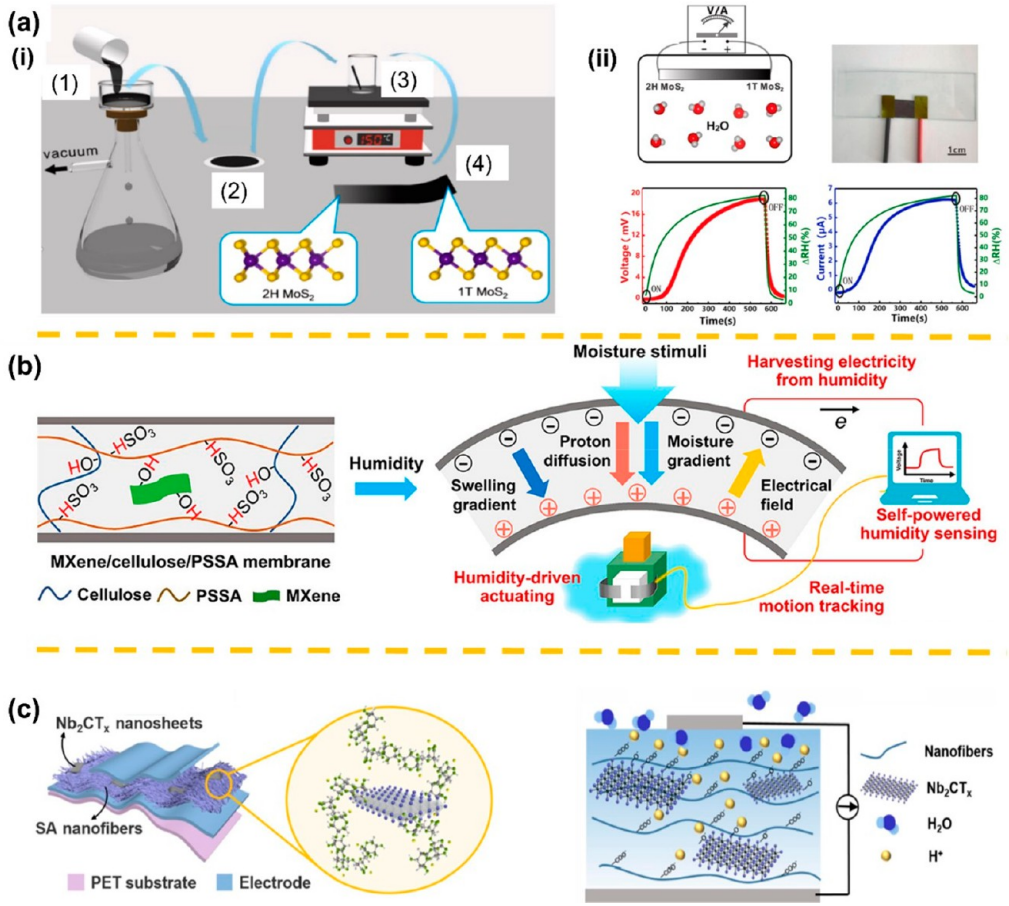

Figure 9. Transition metal based MEGs. (a) (i) Preparation of a 2H−1T MoS_2 sheet. The vacuum-filtered MoS_2 film is thermally annealed to partially transform it from 1T to 2H. (ii) The experimental setup and the corresponding observed results. Reprinted with permission from ref 99. Copyright 2021 Elsevier. (b) A membrane consisting of MXene/PSSA/cellulose is employed in an MEG as the active layer. The terminal surface endows MXene with great hydrophilicity, showing potential in harvesting energy from moisture. Reprinted with permission from ref 100. Copyright 2021 American Chemical Society. (c) Schematic illustration of the conjugation of MXene and SA nanofibers. Reprinted with permission from ref 105. Copyright 2022 Elsevier.

established, subsequently reducing the current and power density output and impeding the device for life-long applications.[87] Thus, a morphology modification avoiding the agglomeration of GO can further promote the corresponding proton conductivity. The recent techniques involve the integration of covalent bonding and proton-conductive materials such as polymer electrolytes.[88,89] However, the intercalation of covalent bonding on GO surfaces is risky because of the possibility of the introduction defects in the GO. To truly facilitate the proton conductivity, such defects are undesirable.

In this manner, Daripa and co-workers noncovalently functionalized GO through the addition of a block copolymer (BCP) to enhance the morphology and eliminate the negative effects of defects. In this study, the hydrophilic BCP, [poly(3-hexythiophene)-*block*-poly (4-styrenesulfonic acid] (P3HT-*b*-PSSA) was anchored on the surface of rGO.[90,91] It was found that insertion of PSSA chains to the rGO sheets helps achieve a good alignment between the adjacent rGO layers. Also, the surface of the graphene sheets is homogeneously covered by the BCP to introduce the porous nanochannels, which was a result of microphase separation from the noncovalently bonded BCP. As such, a proton-conductive network was developed microstructurally. Taking all the advantages into account, a much higher proton conductivity was recorded, up to 0.5 S cm^{-1} compared to that of the pristine GO. Besides, PSSA is hydrophilic owing to the ingredient of sulfonic acid groups. The ion concentration gradient can be easily established between PSSA and rGO upon exposure to moisture, since the oxygen-containing groups have been removed in rGO in advance.

Similarly, Huang et al. developed an active composite material by coupling porous GO and sodium polyacrylate (PAAS) (as shown in Figure 8a).[49] The hybrid structure endows the device with the capability of being used across all regions. Specifically, the proposed MEG can generate electricity in a temperature range of −25 to 50 °C and an RH range from 5% to 95%.[49] The all-region-applicable merit is a consequence of the abundant functional groups within the novel composite. The enormous micropores and hydroscopic functional groups present within the composites assist in the mobile ion generation and boost the ion migration across the interlayers under the ion concentration difference. Taking the advances above into account, a substantial potential of 0.6 V is delivered for 120 h at room temperature.

It is worth noting that the reduction in RH can generally induce the water desorption of the device, resulting in the decay of the electrical signal. Also, the saturation of water absorption in the device can retard the electrical output unless replenishment is conducted by drying out the moisture content

https://doi.org/10.1021/acsanm.2c01557
ACS Appl. Nano Mater. XXXX, XXX, XXX−XXX

in the device.[42,92] Therefore, such a gap period between each cycle of output and drying should be avoided in terms of enhancing the device performance. As such, besides prolonging a single cycle of output duration, efforts are also desired to address the above concerns. Recently, a solution to this bottleneck has been proposed in the form of a SiO_2 nanofiber/sodium alginate (SA)/rGO composite.[93] Instead of working as a proton donor, rGO in the study participated as a skeleton for the composite. Meanwhile, the ionic conductivity of the composite was enhanced by the presence of rGO. As for the proton donor, SA chains can substantially dissociate Na^+ ions in the moist environment. On the other hand, the addition of SiO_2 fibers increases the porosity of the composite, assisting water molecule transportation. Accordingly, the composite is endowed with a great water-adsorbing capacity and diffusion coefficient, leading to a high voltage and current of 0.5 V and 100 μA at an RH of 100%.

More surprisingly, it was found that an unchanged voltage and a current of 50 μA were detected upon exposing the device to an RH of 15%, at which the device was undergoing water desorption.[93] This observation was ascribed to the ion-hydration energy difference. Despite the decreased water content in the system, the dissociated Na^+ ions remain hydrated, and they are surrounded by water molecules. As shown in Figure 8b, during the water desorption process, a water content gradient is constructed, where the region exposed to the environment will have fewer water molecules. In this way, the Na^+ ions have fewer neighboring water molecules in the region with less water content, which is believed to possess a higher ion-hydration energy.[93,94] Conversely, the region with more water content would weaken the relative energy. Governed by the ion-hydration energy difference, the highly "energetic" hydrated ions are driven toward the side with the "inert" ions during the occurrence of water desorption, similar to that of the gradient in ionic concentration. Such a utilization of water desorption in line with water absorption in electricity generation could provide an electrical signal for approximately 240 000 s by varying the RH. Therefore, future attention can be focused on investigating and adopting the proposed mechanism associated with the water desorption process to achieve a sustainable cyclic performance in generating electricity, which is useful for bringing MEGs into reality.

3.2. Transition Metal Materials. Analogous to graphene, TMDCs are emerging 2D nanomaterials that exhibit impressive electrical properties and mechanical flexibility.[95,96] The direct band gap endows TMDCs with advanced potential in optoelectronics.[97,98] TMDCs commonly exist in either a 1T metallic phase or 2T semiconducting phase, which can be turned under certain conditions such as thermal annealing.[97] The adjustable morphology of TMDCs further promotes their application in energy storage and energy generation.

He et al. recently integrated a candidate of TMDC material, molybdenum disulfide (MoS_2), with an MEG that could provide a V_{oc} output of 19 mV and short-circuit current output of 6.24 μA.[99] In contrast to the commonly reported materials, the internal resistance of the MoS_2 film MEG was as low as 3 kΩ. The active layer is composed of stacked MoS_2 nanosheets simply fabricated through a vacuum filtration process, followed by annealing at 150 °C to partially transform the phase on the heated side from the 1T phase to the 2H phase (Figure 9a). As a legacy of the fabrication process, hydrogen ions exist as the residue and are covalently bound with sulfur. Since the 2H MoS_2 surface will release energy during the dissociation process, the residual hydrogen ions detach more easily from the surface instead of from the 1T MoS_2 surface. So, water molecules interact with the dissociated hydrogen ions to form free-state hydronium when penetrating the MoS_2 layer. Thus, an ion concentration gradient is formed, leading to ion migration from the 2H side to the 1T side for electricity generation.

Other than the above-mentioned 2D nanomaterials, transition metal carbide/nitrides, denoted as MXene, have shown great potential in integration with MEGs.[100] The terminal surface of the MXene can contain the oxygen-containing functional groups that are similar to those of GO by selective etching from the MAX phase, which is the precursor of MXene, resulting in an MXene with superior hydrophilicity.[101−103] More importantly, instead of the trade-off between the conductivity and hydrophilicity of other 2D nanomaterials (e.g., GO and MoS_2), MXene can well balance the coexistence of the two characteristics.[101,104] The above-mentioned merits of MXene contribute to its potential application in energy conversion/storage and electronics, which brings a good insight into our study of MXene in MEGs. For example, a combinational compound of MXene/cellulose/PSSA was employed in an MEG and demonstrated the ability to generate electricity upon exposure to moisture, where MXene is ionized into mobile H^+ and works similar to GO (Figure 9b).[100]

The utilization of MXene in MEGs was also studied as a composite with SA.[105] As a control experiment, it was found that the pure SA nanofiber film was incapable of inducing an electrical potential due to low hydrophilicity at low RH. Although the pure SA network displays an electrical signal at elevated RH, a performance saturation occurs at high RH (>70%). It was ascribed to the collapse of the cross-linking between the nanofibers at high RH, generating abundant pathways for extensive water diffusion. Inspired by the neuron-like network, MXene (Nb_2CT_x) was embedded into an SA nanofiber network as a linker to strengthen the network and enhance the water uptake capability simultaneously (Figure 9c). In this way, the integration constructs abundant hydrophilic nanochannels for water absorption and migration, which successfully improves the electrical output from 0.25 V (pure SA nanofibers) to 0.53 V (Nb_2CT_x/SA) at an RH of 91.5%. An optimal power density of 0.6 μW cm^{-2} was achieved by connecting with an external resistance of 64 MΩ.

Interestingly, the hydrogel concept has also been studied in MEGs with the participation of MXene nanosheets.[106] Similar to the neuron-like network, MXene was introduced in a PAM (polyacrylamide) network to form the MXene/PAM hydrogel. This novel design is capable of generating a voltage of 4 mV through absorbing the moisture from human breath.[106] The mechanism can be again explained by the diffusion of the ions dissociated from the functional groups of MXene. Despite the low voltage output, the integration of a hydrogel with 2D nanomaterials needs more future studies. On one hand, a hydrogel owns the features of super hydrophilicity and porous structure, which exhibit potential in MEGs.[107,108] When it comes to the hydrophilic polymeric materials [e.g., PSSA, PVA, poly(ethylene oxide) (PEO), etc.], they can also dissociate mobile ions for assisting electricity generation.[42,109−111] On the other hand, the outstanding electrical performance of 2D nanomaterials can play a role in enhancing the conductivity of

https://doi.org/10.1021/acsanm.2c01557
ACS Appl. Nano Mater. XXXX, XXX, XXX−XXX

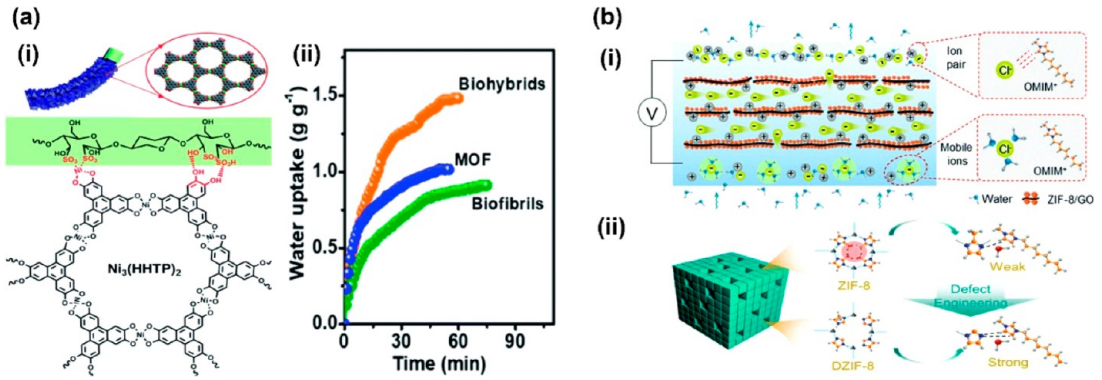

Figure 10. MOF-based MEGs. (a) (i) MOF grown on cellulose biofibrils. (ii) Comparison of the capability of water uptake, demonstrating the high affinity of water absorption of the $Ni_3(HHTP)_2$-decorated biofibrils. Reprinted with permission from ref 125. Copyright 2022 Royal Society of Chemistry. (b) (i) Proposed mechanism of the selective ion permeation for electricity generation. (ii) Schematic illustration of the interaction with the cations dissociated from the IL films for the pristine ZIF-8 and the defected ZIF-8, respectively. Reprinted with permission from ref 92. Copyright 2022 Royal Society of Chemistry.

the hydrogel, potentially resulting in a better output performance.[112,113]

3.3. Metal−Organic Framework (MOF). A MOF is a hybrid organic−inorganic material that exhibits a porous structure.[114] The organic ligands link the metal ions and construct a hollow structure, and thus, MOFs generally possess a high surface area, which is instrumental to the interfacial interaction.[115] With this aid, a MOF is often assembled by different metal ions and organic substances to fabricate sorbents for gases, including atmospheric moisture.[116−118] Due to the high surface porosity and interaction with polar solution, MOFs have been extensively reported to have the capability of harvesting water from the ambient environment.[119−121]

Instead of offering free protons like GO, the employment of MOFs in MEGs is often reported as a modification that boosts the device performance. For instance, 1D materials such as biofibers (e.g., cellulose) are reported for the feasibility in generating electricity upon exposure to moist air flow.[122−124] However, the voltage output is commonly limited to 100−200 mV. For instance, a paper cellulose in MEG was reported with a voltage signal of 0.25 V.[123] Therefore, Han et al. initiated the introduction of a MOF into biofibers, and it was found that the voltage could be improved to 0.66 V at an RH of 99%. More surprisingly, the device could cogenerate water with a production rate of 0.8 g g^{-1} h^{-1}.[125] In the study, sulfonate cellulose nanofibril membranes were decorated with nickel ions and organic ligand linker (e.g., HHTP) through hydrogen bonding (Figure 10a). The addition of the MOF to the biofibril membrane significantly enhances the conductivity, and more importantly, it offers a greater extent of porosity that increases the relevant surface area. The combination of these factors motivates the MOF-based membrane in water absorption (Figure 10a, part ii). As a result, the device governed by the streaming potential offers a better voltage output than the device that consists solely of the biofibrils. Also, the performance is even better with a greater content of the MOF since the capability of the water uptake of the membrane could be further improved.

Besides the scheme of the streaming potential, a MOF was also reported as an assistant in enhancing ion diffusion under a concentration gradient. Recently, an outstanding current density of 1.5 mA cm^{-2} was demonstrated in a MOF/GO membrane, in which zinc ions and 2-methylimidazoe (2-Hmim) were in situ synthesized on the GO skeleton.[92] The membrane was then calcined to introduce defects on the MOF nanoparticles. 1-Octyl-3-methylimidazolium chloride ionic liquid (IL) films were incorporated on the membrane as a mobile-ion donor. Unlike conventional MEGs, the asymmetric exposure of the IL films to moisture could generate numerous ion pairs (cation and anion) simultaneously, which could diffuse under the concentration gradient. Notably, the potential difference could not be induced unless a separation of the ion pairs was achieved. Thus, the MOF membrane plays an important role in realizing the electrical output. It was found that the MOF nanoparticles after calcination are endowed with defects and possess fewer Zn−N bonds, which generates unpaired N-terminals that provide electrons to bind with the cations (Figure 10b, part i). Thus, the cations are bound, and their movements are inhibited due to the strong hydrogen-bond interaction force with the MOF framework (Figure 10b, part ii). Additionally, the enhanced porosity further improves the selective ion permeation within the membrane. Therefore, the electrical output saw a boost in the current and power density compared with those of the GO-based MEGs.

At present, the research of MOFs on MEGs remains at an early stage. Nevertheless, like that of GO, MOFs have become emerging candidates in applications of moist sensors.[126−128] This response upon encountering moisture is attributed to the high affinity with water and high porosity for trapping water molecules.[129,130] Also, MOFs own a great freedom in tunability, and the replacement of the metal ions in the MOF structure could significantly affect the water uptake capability.[131] With the mentioned features, MOFs could be forecast to be a contribution to MEGs in future work.

This section mainly focuses on discussing 2D nanomaterials on MEGs, including graphene-based materials, transition metal materials, and MOFs. Among all, GO is the most widely reported material in MEGs due to its superior functionality. For this reason, various work has also been done on promoting the performance of devices that are assembled with GO. Under the working principle of 2D nanomaterials in MEGs, hydrolysis and ion diffusion are the background of electricity generation. The hydrophilicity of the materials and the capability of ion diffusion are hot topics in terms of device performance. Thus, methods such as element intercalation and acidification treatment are proposed for modifying the proton conductivity and the morphology of the materials. Experiments have also

https://doi.org/10.1021/acsanm.2c01557
ACS Appl. Nano Mater. XXXX, XXX, XXX−XXX

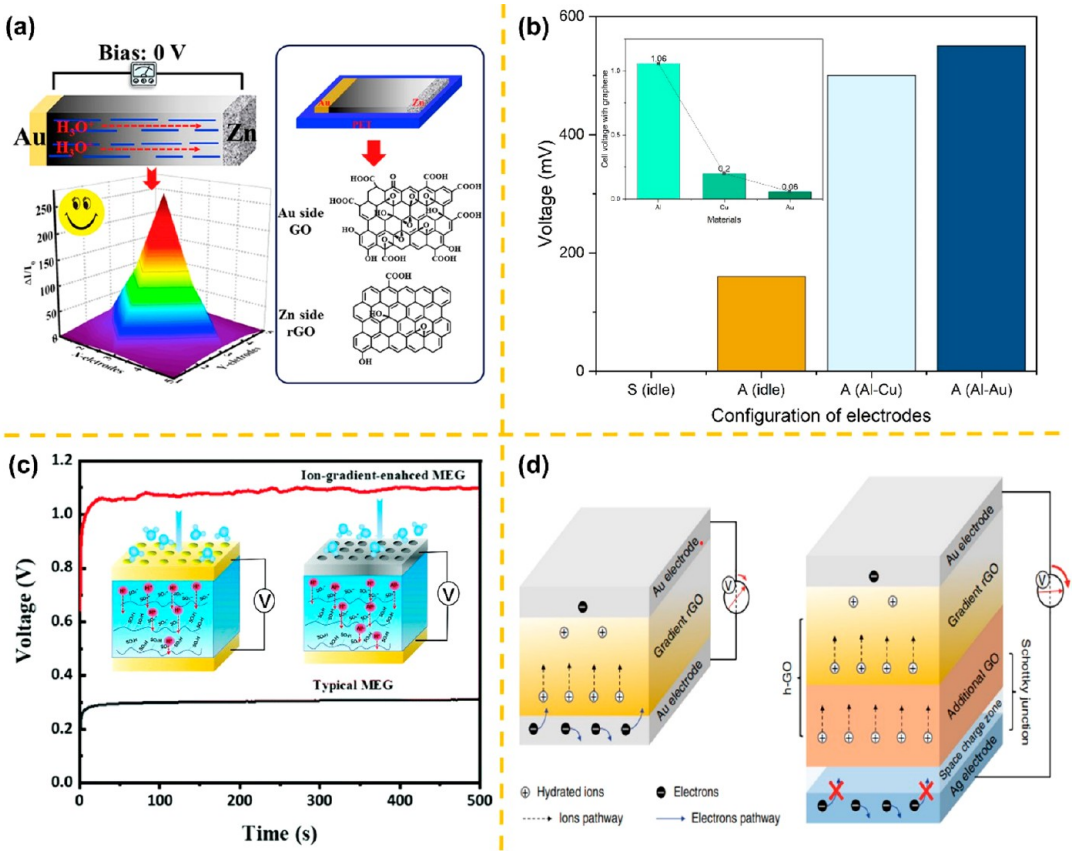

Figure 11. (a) Scheme of the self-assembled MEG with two asymmetric electrodes. The figure (right) shows the transformation of GO into rGO at the Zn site, indicating the occurrence of the electrochemical reaction between the GO and Zn electrode. Reprinted with permission from ref 140. Copyright 2019 Elsevier. (b) The voltage output of the device with a different configuration of electrodes: S, symmetric electrode; A, asymmetric electrodes; idle, at rest in the air without a bias moisture input. The inset shows the cell voltage of metals with graphene, indicating Al is the most active to graphene while Au is inert to graphene. Data is from Hu's work. Reprinted with permission from ref 141. Copyright 2016 Wiley-VCH. (c) The voltage output of the typical MEG (black curve) and the ion-gradient-enhanced MEG (red curve). The inset figure schematically illustrates the structural difference of the two MEGs. Reprinted with permission from ref 143. Copyright 2021 Royal Society of Chemistry. (d) The conventional design of an MEG (left) and the proposed h-GO MEG with asymmetric electrodes (right). Reprinted with permission from ref 47. Copyright 2018 Springer Nature.

been initiated on MoS_2, MXene, and MOFs, which are other emerging candidates for 2D nanomaterials. The observed results further verify the feasibility of 2D nanomaterials in MEGs. However, due to the finite work reported for other 2D nanomaterials in MEGs, the approaches to boost the performance of the corresponding device are yet to be explored. Also, more 2D nanomaterials deserve investigation as those in other water-induced electricity generators. For instance, droplet/flow-induced electricity that is governed by the electrokinetic theory has been extensively reported with graphene as the participant.[132−134] Compared with the semiconductive-like GO, the employment of graphene might result in a better output due to the extraordinary electrical conductivity.[135] Likewise, even though pristine hexagonal boron nitride (hBN) stays hydrophobic in nature, the intrinsic high ζ-potential could be a booster to allow the contributions of hBN in MEGs.[136,137] Therefore, these materials could share a similar promise with the aforementioned 2D nanomaterials in MEGs.

4. ARCHITECTURE OF MEGS

4.1. Role of Electrodes in MEGs. Most of the current research focuses on the development of the active materials in MEGs or the architecture of MEGs, but limited work has been done on studying the role of electrodes in MEGs. However, the existing studies related to electrodes have significantly proven the importance of the connection electrodes in either realizing or boosting the performance of MEGs.

The electrochemical reaction is found to occur when an active metal (e.g., Al and Cu) is attached to GO. In contrast, those metals inert to GO (e.g., Au) stay stable in contact with GO.[138,139] This provides a new insight into constructing the ion concentration gradient in GO. Therefore, Zhang et al. utilized the concept of the redox potential to fabricate an MEG device without the complex ECT process, as shown in Figure 11a.[140] In this device, GO film is deposited between two metallic electrodes, one of which is the active metal such as Zn, Cu, and Al, while the other is the inert metal such as Au. The reaction between GO and the Au electrode is negligible, which is attributed to the low redox potential of GO, but the oxygen-containing groups can be significantly removed at the side close to the active metal, and thus GO is reduced.[140] In this regard, a gradient of oxygen-containing groups is established in which an asymmetric ion concentration is formed for further ion migration. Since the oxygen-containing groups such as epoxide are extremely unstable at high temperature, the strategy readily solves the limitation of the uncontrollable reduction of GO through thermal annealing.

https://doi.org/10.1021/acsanm.2c01557
ACS Appl. Nano Mater. XXXX, XXX, XXX−XXX

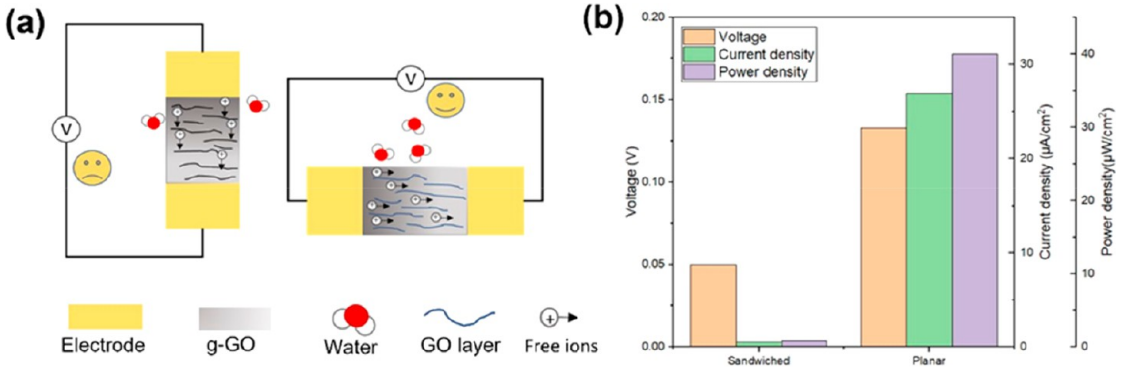

Figure 12. (a) Schematic of the sandwiched and planar structures of MEGs. With the example of GO, mobile protons are less plugged in the migration within the configuration. (b) Electrical output of MEGs in the sandwiched and planar configurations; data is from Zhang's work. Reprinted with permission from ref 140. Copyright 2019 Elsevier.

Moreover, the configuration of electrodes is crucial in enhancing the output of MEGs. Experimental work was conducted to compare the symmetric electrodes (Al−GO−Al) and the asymmetric electrodes (Al−GO−Au).[141] A summary of the electrical performance is shown in Figure 11b. The electrochemical reaction between the active metal (Al) and GO will be triggered by moisture. However, the reaction occurs simultaneously at the symmetric electrodes, which offsets the output voltage, owing to the opposite polarity, and results in a total of 0 V. As for the asymmetric electrodes, the inertness of Au to GO stymies the electrochemical process, which happens solely on the side of the Al electrode. As a result, an ion concentration gradient develops across the device, which can output a voltage of up to 160 mV.

Furthermore, the asymmetrical configuration also upgrades the level of output. The V_{oc} of the devices composed of Al−GO−Cu and Al−GO−Au are ±500 and ±550 mV, respectively. Al/GO demonstrates the largest potential gap while that of Au/GO is the smallest among the tested samples, which is attributed to the energy gap between the corresponding metals and GO.[138,142] In the case of placing the MEG in a moist environment without applying a bias externally, the total output voltage is summed up by the individual outputs at each electrode. Thus, the MEG with the structure of Al−GO−Au offers a greater magnitude in electrical output.[141] The observation is also verified in a fiber-based MEG coupled with asymmetric electrodes, where the active metal (Al) and a relatively inert metal (Cu) serve as the top and bottom electrodes, respectively, as shown in Figure 11c.[143] The mobile hydrogen ions generated from the sandwiched active materials tend to react with the active top electrode and release additional metallic ions. The invention provides more mobile ions within the device, contributing to the further development of the ion concentration gradient.

The role of the asymmetric electrodes in enhancing the performance of the MEG was further studied in Huang's work. A device composed of Ag/GO-gradient reduced GO (grGO)/Au demonstrates the capability of approaching a V_{oc} of 1.5 V, which was the optimal level compared to those of other MEGs of that era.[47] Figure 11d shows that, in the architecture of the pre-existing MEGs, electrons may escape from the bottom electrode and migrate toward the upper electrode, where the moving positive ions can be neutralized by the passing electrons. It results in eliminating the extent of an ion concentration gradient. However, this phenomenon is not found in the proposed device. Electrons are confined at the bottom electrode, and only protons are movable along with the gradient. The Fermi energies of Ag, GO, grGO, and Au are 4.3, 4.9, 4.4−4.7, and 5.1 eV, respectively. When Ag contacts with GO (4.3−4.9 eV), it shows a tendency to realize a Schottky diode characteristic.[47,49] In contrast, grGO and Au (4.4−4.7 to 5.1 eV) complete an ohmic contact. The entire circuit restricts the electrons to a unidirectional flow and prevents the recombination of electrons and protons. If symmetric electrodes are employed in this device, the electrical output is dramatically decreased due to the clash of the two same junctions. Thus, the messy flow of charges descends the electrical output. Since Schottky contact is commonly found between a metal and semiconductor, the principle is believed to be applicable on the device consisting of MoS_2. Therefore, apart from studying the functionality of the active layer, it is also worth exploiting the capability of electrodes to enhance the performance of MEGs.

4.2. Configuration of MEGs. All of the proposed MEGs have the same structure of electrode/functional layer/electrode, and they can be categorized into two groups, either a planar or sandwiched configuration. As shown in Figure 12a (left), the sandwiched structure has two electrodes in the vertical direction and an active layer placed between them. Generally, the ion concentration gradient is also constructed in the same orientation, while the planar structure has everything in the horizontal direction.

Under the working principles of MEGs, migration of ions is dominant in determining the performance of the device. Therefore, any obstacles that might hinder ion movement could decrease the electrical output. The concern could be more significant for active materials with a lamellar structure. In the case of sandwiching GO with top and bottom electrodes, the pathway of the hydrolyzed protons is distributed vertically. However, GO film is a stack of multiple layers of nanosheets, which tend to obstruct the movement of the mobile ions across the vertical direction,[57] as illustrated in Figure 12a. Therefore, GO has poor conductivity in the out-of-plane direction, and the movement of ions requires large energy as well.[140] Thus, the output is not maximized. This drawback could be improved by transforming the device into a planar configuration. Figure 12b depicts the comparison of the electrical output of the device in the sandwiched and planar structures. With the ion concentration gradient across the horizontal direction, ions move in the barrier-free pathway, and therefore, the overall efficiency of charge transportation increases such that the electrical output can be enhanced.

https://doi.org/10.1021/acsanm.2c01557
ACS Appl. Nano Mater. XXXX, XXX, XXX−XXX

Table 2. Summary of MEGs

active material	electrode	configuration	RH value (%)	electrical output	ref
GQD	Au	planar	70	0.27 V, 1.86 mW/cm^2	43
g-GOF	Au	sandwiched	30	0.035 V, 0.42 μW/cm^2	46
GOF	Au	sandwiched	70	0.7 V, 27 μW/cm^2	77
GOF	Au	sandwiched	70	0.7 V, 25 μA/cm^2	55
GOF	Au/Zn	planar	95	0.13 V, 43 mW/cm^2	140
GO fiber	rGO	planar	65	0.35 V, 1.06 mW/cm^2	75
g-GO	Au	sandwiched	85	0.45 V, 2.02 μW/cm^2	48
OG/FOG		sandwiched	60	0.75 V, 9 μW/cm^2	78
GO	Pt	sandwiched	80	6.2 μA/cm^2, 0.07 μW/cm^2	54
GO	FTO/Ag	sandwiched	75	0.85 V, 92.8 μA/cm^2	82
GO	Ag	sandwiched	10	1.2 V, 2.5 μW/cm^2	84
rGO/BCP	Ag	sandwiched	94	6.40 μA/cm^2, 1.15 μW/cm^2	90
GO/PAAS	Au/Ag	sandwiched	5−95	0.2−0.6 V, 0.07 μW/cm^2	49
SA/SiO_2 nanofibers/rGO	Au	sandwiched	100	0.5 V, 100 μA	93
			15	0.5 V, 50 μA	
GO/rGO	Ag/Au	sandwiched	80	1.52 V, 32 mW/cm^2	47
GO	rGO	planar	60	0.07 V, 12 mA/cm^2	57
MoS_2	Cu	sandwiched	80	0.019 V, 6.24 μA	99
$Ti_3C_2T_x$/PSSA/cellulose	AgNWs	sandwiched	80	0.3 V, 81.2 μW/cm^3	100
Nb_2CT_x/SA nanofibers	Au/Ni−Cr	sandwiched	91.5	0.53 V, 0.5 μW/cm^2	105
paper cellulose	stainless steel	sandwiched	70	0.25 V, 10 nA/cm^2	123
$Ni_2(HHTP)_3$/biofibrils cellulose	carbon-plated Al	sandwiched	99	0.66 V, 150 nA/cm^2	125
ZIF-8/GO	Ag/AgCl	sandwiched	37	0.3 V, 1.5 mA/cm^2	92

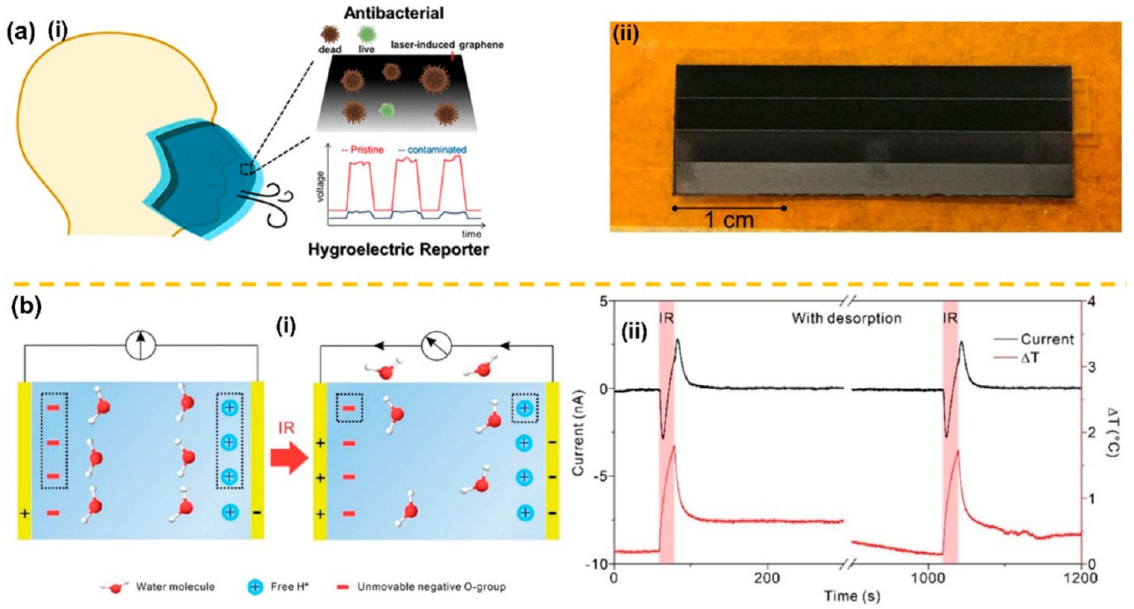

Figure 13. (a) Scheme illustration of the LIG film-based mask. (i) The LIG film is embedded into the commercial mask as a replacement for the molten-blown fabric. The curve shows the voltage output of the device with the intake of contamination. (ii) The scheme shows the photograph of the LIG film. The gradual color change depicts the degree of oxidation within the LIG film, where the number of oxygen-containing groups increases from the dark to gray regions. Reprinted with permission from ref 144. Copyright 2020 American Chemical Society. (b) (i) Working principle of the MEG-based IR detector. (ii) The curve demonstrates the change in the electrical output of the detector upon encountering IR light. Reprinted with permission from ref 147. Copyright 2020 Royal Society of Chemistry.

In a short summary, existing studies have demonstrated the correlation of the architecture of MEGs with device performance. First, asymmetric electrodes are more favorable for electricity generation since they assist in constructing a greater ion concentration gradient and confining the charge migration. Furthermore, switching from a sandwich to a planar structure can considerably alleviate the disadvantage of ion transport difficulty in active materials having a lamellar structure. However, limited work has been done on researching the architecture of MEGs based on materials other than GO. Therefore, future studies are necessary to verify the proposals on more applicable materials. As a summary, Table 2 provides an overview of the information regarding the recently reported MEGs.

https://doi.org/10.1021/acsanm.2c01557
ACS Appl. Nano Mater. XXXX, XXX, XXX−XXX

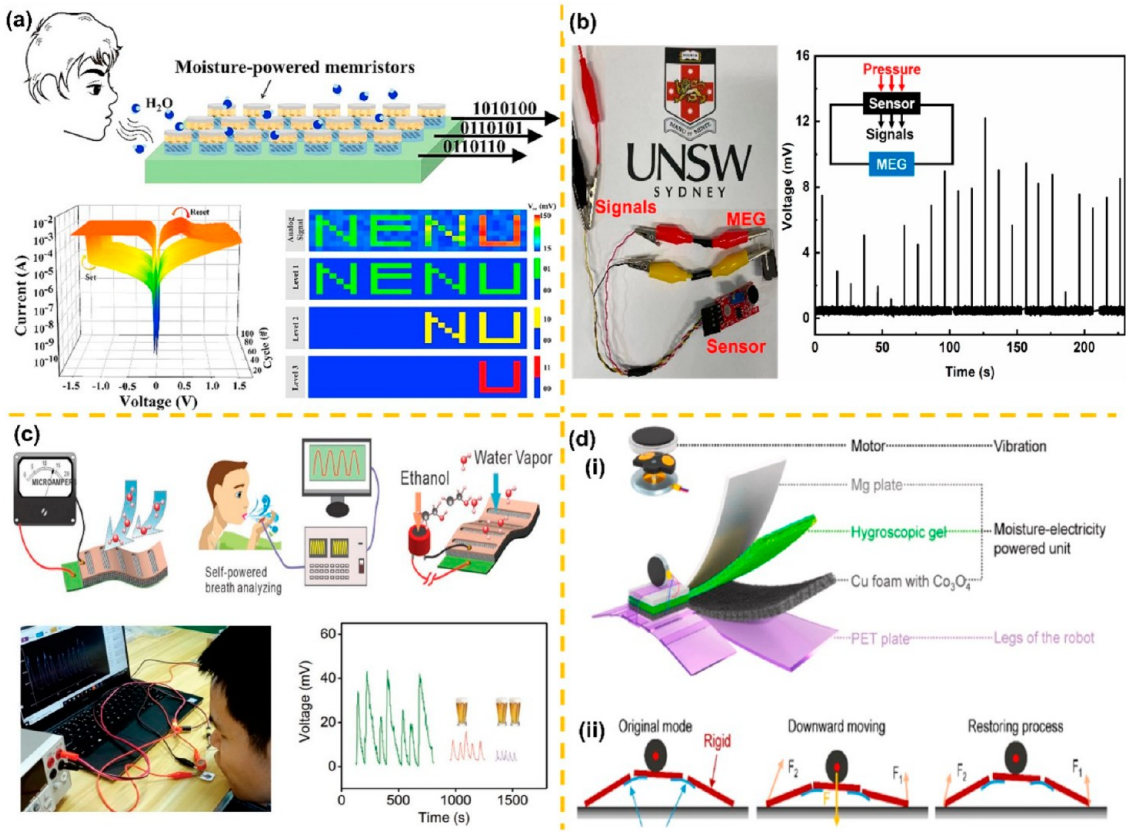

Figure 14. (a) Array of an 8 × 8 unit memristor powered by an MEG. The output voltage is varied at each unit that could be transformed for information storage. Reprinted with permission from ref 150. Copyright 2020 Elsevier. (b) A pressure sensor driven by the GO-based MEG. Reprinted with permission from ref 82. Copyright 2022 Elsevier. (c) The integration of an ethanol detector with a TiO_2 NWs-based MEG. Measurement of the ethanol concentration in human exhalation is displayed as a voltage output of the MEG. The voltage output is varied when the internal resistance of the ethanol detector is impacted by the ethanol concentration. Reprinted with permission from ref 151. Copyright 2019 Wiley-VCH. (d) (i) Assembly of the cockroach-like microrobot driven by an MEG. (ii) Illustration of the mechanical motion of the MEG robot. The robot is driven forward by the consecutive elastic stretching of the flexible PET plate by the vibrational motion. Reprinted with permission from ref 152. Copyright 2021 Elsevier.

5. APPLICATIONS

The applications of MEGs can be classified into two groups, as either a "sensor" or a "power supply". The sensor terminology refers to devices that are strongly reliant on moisture absorption and realize functions based on different moisture absorptions, in which detectors are good examples. Conversely, the power supply system refers to those that work as a power supply and transfer the generated output to external devices.

5.1. Sensors. The COVID-19 pandemic has significantly affected our life. To better protect us from infections, the world health organization (WHO) has suggested the importance of the facial mask. Considering the safety issue, the condition of a used mask is the biggest subject of concern. The solution to this was invented by Huang's team, by incorporating the concept of an MEG in a commercial surgical mask as shown in Figure 13a.[144] A layer of gradient laser-induced graphene (g-LIG) that is obtained through laser irradiation of polyimide (PI) under a CO_2 environment becomes an alternative to the layer of melt-blown fabric in the mask.[145,146] The g-LIG film demonstrates the capability of blocking bacteria as well as monitoring the lifetime condition of the mask.[144] Note that an additional round of laser irradiation is introduced to oxidize the pristine graphene film into GO and establish a region of gradient GO by modulating the degree of lasing gradually. The moisture from the inhalation and exhalation of humans is used to generate electricity. However, with the intake of contaminants, the gradient in the GO collapses, which is reflected by the change in voltage output. There is an outstanding drop in the voltage as the amount of adhered bacteria increases.

As to the application of MEGs in detectors, it has been suggested that MEGs are promising as tactile detectors, humidity detectors, and breathing detectors.[46,57,135] Recently, the concept of MEGs in detectors has also expanded into the detection of infrared (IR) light, as shown in Figure 13b.[147] Initially, a positive voltage is generated when the GO device is exposed to moisture. Upon further intake of moisture, the device becomes saturated since the electric field is stronger to balance the charges induced by the ionization of the functional groups. Fewer charges then need to be balanced by the external circuit, consequently causing a voltage drop. Thus, the output remains at zero unless further environmental changes are detected. When IR light is emitted to the device, the intrinsic thermal energy is absorbed by the water molecules that exist in the GO, which are then activated vibrationally. This results in water desorption from the GO, leading to a demand in the external circuit to balance the polarized charges. Consequently, a significant positive peak that indicates the output generation could be observed over the zero line.

https://doi.org/10.1021/acsanm.2c01557
ACS Appl. Nano Mater. XXXX, XXX, XXX−XXX

5.2. Power Supplies. MEGs can also work as an energy supply to drive a wide range of small electronics, such as commercial calculators, LEDs, monitors, etc. These fields of application have been widely verified since they are commonly employed as volunteers to evaluate the performance of the MEGs. In the case where the application requires high power input, the MEG can be connected to a capacitor for storing the generated electricity. The pathway is validated to trigger energy generation and storage simultaneously when a supercapacitor is hybridized with an MEG, where a voltage of 0.2 V and charge of 870 mC cm^{-3} is generated in an individual device.[148] The energy storage is expected to be improved when the scale of connection increases to 10 devices.

It would be extremely useful if MEGs could cope with the demand for information applications, as our daily lives rely heavily on data. The memristor that is used to store and process information is a crucial component in telecommunication. Noticing this, Zhao's team developed a GO-based MEG-driven memristor which harvests energy from human breath.[149] This is also validated by a power-free memristor device developed by Tao et al. that integrates power generation and resistive switching (RS) merits in one device, as shown in Figure 14a.[150] By capturing the moisture from human breath, voltage is generated. Regarding the voltage magnitude, RS functionality was achieved and "NENU" was displayed by a standard eight-bit ASCII when the team constructed an 8 × 8 array using the proposed device. Similarly, the GO-based MEG could supply adequate energy to power up the pressure sensor.[82] As shown in Figure 14b, the connected pressure sensor could reflect the response by means of an electrical signal.

Besides, applications as power sources developed from other-dimensional material-based MEGs could also be used as references for prospective studies of 2D nanomaterial-based MEGs. For instance, a TiO_2 nanowires (NWs)-based MEG was studied in a healthcare application, of which an ethanol sensor was powered to monitor the health of humans through breathing (Figure 14c). The unhealthy condition brings changes to the exhalation of humans, and the monitor notices the changes and sends out signals for warning.[151] In line with the trend of the development in robots, a cockroach-like microrobot that could be powered for locomotion was reported through integration with an MEG (illustrated in Figure 14d).[152] The MEG unit converts the captured moisture into electricity, which is then transmitted to the connected motor. When the motor is powered up, vibrational motion is supplied to continuously stretch the flexible PET plate to drive the robot forward. Therefore, an insight could be given on the application of MEGs in artificial intelligence, which is an emerging topic.

With years of research in achieving a substantial electrical output, MEGs have shown great potential in commercial applications. As a new-generation power source, MEGs could work as either a power supply or a sensor upon exposure to moisture. As to that of the sensor, MEGs could output monitoring signals based on the changes of moisture, while MEGs could also induce electricity and power the external components, e.g., memory devices and healthcare products. To further functionalize the device, capacitors could be adopted for energy storage. Besides, the compacted structure of MEGs assists in the size minimization of the applicable devices for practical applications. Since moisture is ubiquitous in ambient conditions, the applications of MEGs could be further expanded across the daily field. Therefore, future insights could be poured into a hybrid of MEGs with other sources of natural energy such as solar energy and raindrops. These efforts are believed to be necessary to construct an alternative device to the battery that is capable of working in all regions and all day.

6. CONCLUSION AND PROSPECTS

In conclusion, we have summarized the recent advances in MEGs, particularly focusing on 2D nanomaterials in MEGs. The existing achievements of MEGs have been summarized as well. The contents of this work are discussed across the aspects of working principles, materials, and potential applications. In summary, there are two working principles for MEGs, the ion concentration gradient and the streaming potential, of which 2D nanomaterials are more reported with the first one according to current studies. In this case, electricity generation in MEGs is attributed to the dissociation of hydrophilic functional groups in the interaction with moisture. Through the discussion on the progress of MEGs, it is notable that the output of MEGs can be either transient or continuous, where insight is put on developing the latter one since it offers greater freedom in long-term usage. So far, the developed MEGs have been successfully used in a variety of applications ranging from information storage to healthcare monitoring, artificial intelligence, and wearable electronics. Furthermore, this work also demonstrates the advantage and potential of 2D nanomaterials over other nanomaterials in being engineered for a greater functionality in MEGs.

However, further studies are still necessary, as the unsatisfactory performance of the known MEGs reveals they are still at an infantile stage. The challenges are subject but not limited to the following: (1) There is insufficient knowledge of the working principles, as the mechanism is always the background before comprehensive study about the methods. (2) Low conversion efficiency, which is more related to the material itself, results in a low energy output and short duration of output. (3) A trade-off exists between the performance and the ease of production. Those MEGs that demonstrate strong electrical output might require complicated post-treatments (e.g., additional ion intercalation). Conversely, a pristine sample without treatment could be limited to low output. (4) Studies related to the architecture of MEGs are limited, especially the role of electrodes in MEGs. In addition, there is a lack of research synchronized with active materials, for instance, the verification of asymmetric electrodes in the system of transition metal based MEGs.

The most common approach to overcome the challenges and realize high electrical output for practical applications is through the serial/parallel connection of several devices. But indeed, it brings difficulty in device miniaturization. According to the current research conducted on MEGs, the state-of-the-art techniques in overcoming the challenges are (1) modulation of the active materials to facilitate proton conductivity and ion migration, (2) increasing the number of mobile ions by integrating diverse hydrophilic materials into one device, and (3) selection of the proposed structure, planar over sandwiched, as the latter one hinders ion movement through the interlayer. Notably, more approaches need to be explored on optimizing the performance of MEGs. Though 2D nanomaterials demonstrate great potential in MEGs, most of the current research in MEGs is still limited to graphene-based nanomaterials. The studies of transition metals and MOFs in

https://doi.org/10.1021/acsanm.2c01557
ACS Appl. Nano Mater. XXXX, XXX, XXX−XXX

this field are still in infancy. Aside from developing the existing materials, future studies can be focused on exploring novel 2D nanomaterials for MEGs. One the other hand, the conjugation of 2D nanomaterials with other materials (e.g., hydrogels) is also deserving of endeavor. The hybridization is believed to endow MEGs with diverse functionalities. Additionally, in line with future commercial applications, printing techniques could be regarded as a facile way to realize large-scale production. With more research conducted in the future, the potential of MEGs can be explored, and practical daily applications will be seen one day.

AUTHOR INFORMATION

Corresponding Author

Tao Wan − *School of Materials Science and Engineering, University of New South Wales, Sydney, New South Wales 2052, Australia;* orcid.org/0000-0001-9345-8624; Email: tao.wan@unsw.edu.au

Authors

Ziheng Feng − *School of Materials Science and Engineering, University of New South Wales, Sydney, New South Wales 2052, Australia*

Guangyu Hu − *School of Materials Science and Engineering, University of New South Wales, Sydney, New South Wales 2052, Australia*

Renbo Zhu − *School of Materials Science and Engineering, University of New South Wales, Sydney, New South Wales 2052, Australia*

Shuo Zhang − *School of Materials Science and Engineering, University of New South Wales, Sydney, New South Wales 2052, Australia*

Chao Liu − *School of Materials Science and Engineering, University of New South Wales, Sydney, New South Wales 2052, Australia*

Peiyuan Guan − *School of Materials Science and Engineering, University of New South Wales, Sydney, New South Wales 2052, Australia;* orcid.org/0000-0003-2441-864X

Mengyao Li − *School of Materials Science and Engineering, University of New South Wales, Sydney, New South Wales 2052, Australia*

Haolan Xu − *Future Industries Institute, UniSA STEM, University of South Australia, Adelaide, South Australia 5095, Australia;* orcid.org/0000-0002-9126-1593

Dewei Chu − *School of Materials Science and Engineering, University of New South Wales, Sydney, New South Wales 2052, Australia;* orcid.org/0000-0003-4581-0560

Complete contact information is available at: https://pubs.acs.org/10.1021/acsanm.2c01557

Notes

The authors declare no competing financial interest.

ACKNOWLEDGMENTS

The authors would like to acknowledge the financial support from the Australian Research Council, projects LP210200495, LP190100829, and DP210100879.

REFERENCES

(1) Li, Q. H.; Jin, X.; Yang, Y.; Wang, H. N.; Xu, H. J.; Cheng, Y. Y.; Wei, T. H.; Qin, Y. C.; Luo, X. B.; Sun, W. F.; Luo, S. L. $Nd_2(S, Se, Te)_3$ Colloidal Quantum Dots: Synthesis, Energy Level Alignment, Charge Transfer Dynamics, and Their Applications to Solar Cells. *Adv. Funct. Mater.* **2016**, *26* (2), 254−266.

(2) Hu, L.; Peng, J.; Wang, W. W.; Xia, Z.; Yuan, J. Y.; Lu, J. L.; Huang, X. D.; Ma, W. L.; Song, H. B.; Chen, W.; Cheng, Y. B.; Tang, J. Sequential Deposition of $CH_3NH_3PbI_3$ on Planar NiO Film for Efficient Planar Perovskite Solar Cells. *ACS Photonics* **2014**, *1* (7), 547−553.

(3) Hu, L.; Zhang, Z.; Patterson, R. J.; Shivarudraiah, S. B.; Zhou, Z.; Ng, M.; Huang, S.; Halpert, J. E. PbSe Quantum Dot Passivated Via Mixed Halide Perovskite Nanocrystals for Solar Cells With Over 9% Efficiency. *Solar RRL* **2018**, *2* (12), 1800234.

(4) Valtchev, S.; Almeida, J.; Teixeira, J. P.; Ben Klaassens, J. Conversion of Wind-Induced Vibrations into Electricity. *IEEE 36th International Telecommunications Energy Conference*, Vancouver, Canada, September 28−October 2, 2014; pp 1−8.

(5) Dincer, F. The analysis on wind energy electricity generation status, potential and policies in the world. *Renew. Sust. Energy Rev.* **2011**, *15* (9), 5135−5142.

(6) Li, X. M.; Shen, C.; Wang, Q.; Luk, C. M.; Li, B. W.; Yin, J.; Lau, S. P.; Guo, W. L. Hydroelectric generator from transparent flexible zinc oxide nanofilms. *Nano Energy* **2017**, *32*, 125−129.

(7) Das, S. S.; Kar, S.; Anwar, T.; Saha, P.; Chakraborty, S. Hydroelectric power plant on a paper strip. *Lab Chip* **2018**, *18* (11), 1560−1568.

(8) Salter, S. H. Wave power. *Nature* **1974**, *249* (5459), 720−724.

(9) Alvarez, X.; Valero, E.; de la Torre-Rodriguez, N.; Acuna-Alonso, C. Influence of Small Hydroelectric Power Stations on River Water Quality. *Water* **2020**, *12*, 312.

(10) Wang, Z. L.; Song, J. Piezoelectric nanogenerators based on zinc oxide nanowire arrays. *Science* **2006**, *312* (5771), 242−246.

(11) Yin, J.; Li, X.; Yu, J.; Zhang, Z.; Zhou, J.; Guo, W. Generating electricity by moving a droplet of ionic liquid along graphene. *Nat. Nanotechnol.* **2014**, *9* (5), 378−383.

(12) Dhiman, P.; Yavari, F.; Mi, X.; Gullapalli, H.; Shi, Y.; Ajayan, P. M.; Koratkar, N. Harvesting Energy from Water Flow over Graphene. *Nano Lett.* **2011**, *11* (8), 3123−3127.

(13) Zhao, Y.; Song, L.; Deng, K.; Liu, Z.; Zhang, Z.; Yang, Y.; Wang, C.; Yang, H.; Jin, A.; Luo, Q.; Gu, C.; Xie, S.; Sun, L. Individual Water-Filled Single-Walled Carbon Nanotubes as Hydroelectric Power Converters. *Adv. Mater.* **2008**, *20* (9), 1772−1776.

(14) Yin, J.; Zhang, Z.; Li, X.; Yu, J.; Zhou, J.; Chen, Y.; Guo, W. Waving potential in graphene. *Nat. Commun.* **2014**, *5* (1), 3582.

(15) Li, X.; Shen, C.; Wang, Q.; Luk, C. M.; Li, B.; Yin, J.; Lau, S. P.; Guo, W. Hydroelectric generator from transparent flexible zinc oxide nanofilms. *Nano Energy* **2017**, *32*, 125−129.

(16) Xue, G. B.; Xu, Y.; Ding, T. P.; Li, J.; Yin, J.; Fei, W. W.; Cao, Y. Z.; Yu, J.; Yuan, L. Y.; Gong, L.; Chen, J.; Deng, S. Z.; Zhou, J.; Guo, W. L. Water-evaporation-induced electricity with nanostructured carbon materials. *Nat. Nanotechnol.* **2017**, *12* (4), 317−321.

(17) Zhou, X.; Zhang, W.; Zhang, C.; Tan, Y.; Guo, J.; Sun, Z.; Deng, X. Harvesting Electricity from Water Evaporation through Microchannels of Natural Wood. *ACS Appl. Mater. Interfaces* **2020**, *12* (9), 11232−11239.

(18) Zhao, T.; Hu, Y.; Zhuang, W.; Xu, Y.; Feng, J.; Chen, P.; Peng, H. A Fiber Fluidic Nanogenerator Made from Aligned Carbon Nanotubes Composited with Transition Metal Oxide. *ACS Mater. Lett.* **2021**, *3* (10), 1448−1452.

(19) Bai, J.; Huang, Y.; Cheng, H.; Qu, L. Moist-electric generation. *Nanoscale* **2019**, *11* (48), 23083−23091.

(20) Novoselov, K. S.; Geim, A. K.; Morozov, S. V.; Jiang, D.; Zhang, Y.; Dubonos, S. V.; Grigorieva, I. V.; Firsov, A. A. Electric Field Effect in Atomically Thin Carbon Films. *Science* **2004**, *306* (5696), 666−669.

(21) Grigorenko, A. N.; Polini, M.; Novoselov, K. S. Graphene plasmonics. *Nat. Photonics* **2012**, *6* (11), 749−758.

(22) Stoller, M. D.; Park, S. J.; Zhu, Y. W.; An, J. H.; Ruoff, R. S. Graphene-Based Ultracapacitors. *Nano Lett.* **2008**, *8* (10), 3498−3502.

(23) Zhu, Y. Z.; Wan, T.; Guan, P. Y.; Wang, Y. T.; Wu, T.; Han, Z. J.; Tang, G. C.; Chu, D. W. Improving thermal and electrical stability of silver nanowire network electrodes through integrating graphene oxide intermediate layers. *J. Colloid Interface Sci.* **2020**, *566*, 375−382.
(24) Wang, Q. H.; Kalantar-Zadeh, K.; Kis, A.; Coleman, J. N.; Strano, M. S. Electronics and optoelectronics of two-dimensional transition metal dichalcogenides. *Nat. Nanotechnol.* **2012**, *7* (11), 699−712.
(25) Wilson, J. A.; Yoffe, A. D. Transition Metal Dichalcogenides Discussion and Interpretation of Observed Optical, Electrical and Structural Properties. *Adv. Phys.* **1969**, *18* (73), 193−335.
(26) Kuc, A.; Zibouche, N.; Heine, T. Influence of quantum confinement on the electronic structure of the transition metal sulfide TS_2. *Phys. Rev. B* **2011**, *83*, 245213.
(27) Zhang, K. L.; Feng, Y. L.; Wang, F.; Yang, Z. C.; Wang, J. Two dimensional hexagonal boron nitride (2D-hBN): synthesis, properties and applications. *J. Mater. Chem. C* **2017**, *5* (46), 11992−12022.
(28) Bao, J.; Edwards, M.; Huang, S. R.; Zhang, Y.; Fu, Y. F.; Lu, X. Z.; Yuan, Z. C.; Jeppson, K.; Liu, J. Two-dimensional hexagonal boron nitride as lateral heat spreader in electrically insulating packaging. *J. Phys. D: Appl. Phys.* **2016**, *49*, 265501.
(29) Weng, Q. H.; Wang, X. B.; Wang, X.; Bando, Y.; Golberg, D. Functionalized hexagonal boron nitride nanomaterials: emerging properties and applications. *Chem. Soc. Rev.* **2016**, *45* (14), 3989−4012.
(30) Yang, J.; Zeng, Z. Y.; Kang, J.; Betzler, S.; Czarnik, C.; Zhang, X. W.; Ophus, C.; Yu, C.; Bustillo, K.; Pan, M.; et al. Formation of two-dimensional transition metal oxide nanosheets with nanoparticles as intermediates. *Nat. Mater.* **2019**, *18* (9), 970−976.
(31) Kumbhakar, P.; Gowda, C. C.; Mahapatra, P. L.; Mukherjee, M.; Malviya, K. D.; Chaker, M.; Chandra, A.; Lahiri, B.; Ajayan, P. M.; Jariwala, D.; et al. Emerging 2D metal oxides and their applications. *Mater. Today* **2021**, *45*, 142−168.
(32) Cui, C.; Xue, F.; Hu, W.-J.; Li, L.-J. Two-dimensional materials with piezoelectric and ferroelectric functionalities. *npj 2D Mater. Appl.* **2018**, *2* (1), 18.
(33) Aji, A. S.; Nishi, R.; Ago, H.; Ohno, Y. High output voltage generation of over 5 V from liquid motion on single-layer MoS_2. *Nano Energy* **2020**, *68*, 104370.
(34) Tao, H.; Fan, Q.; Ma, T.; Liu, S.; Gysling, H.; Texter, J.; Guo, F.; Sun, Z. Two-dimensional materials for energy conversion and storage. *Prog. Mater. Sci.* **2020**, *111*, 100637.
(35) Forouzandeh, P.; Pillai, S. C. Two-dimensional (2D) electrode materials for supercapacitors. *Mater. Today: Proc.* **2021**, *41*, 498−505.
(36) Sarmah, H. J.; Mohanta, D. Revisiting principles, practices and scope of technologically relevant 2D materials. *J. Mater. Res.* **2021**, *36* (10), 1961−1979.
(37) Liu, H.; Na, W.; Liu, Z.; Chen, X.; Su, X. A novel turn-on fluorescent strategy for sensing ascorbic acid using graphene quantum dots as fluorescent probe. *Biosens. Bioelectron.* **2017**, *92*, 229−233.
(38) Xiao, S.; Zhou, D.; Luan, P.; Gu, B.; Feng, L.; Fan, S.; Liao, W.; Fang, W.; Yang, L.; Tao, E.; Guo, R.; Liu, J. Graphene quantum dots conjugated neuroprotective peptide improve learning and memory capability. *Biomaterials* **2016**, *106*, 98−110.
(39) Kral, P.; Shapiro, M. Nanotube electron drag in flowing liquids. *Phys. Rev. Lett.* **2001**, *86* (1), 131−134.
(40) Shen, D.; Duley, W. W.; Peng, P.; Xiao, M.; Feng, J. Y.; Liu, L.; Zou, G. S.; Zhou, Y. N. Moisture-Enabled Electricity Generation: From Physics and Materials to Self-Powered Applications. *Adv. Mater.* **2020**, *32*, 2003722.
(41) Xue, J. L.; Zhao, F.; Hu, C. G.; Zhao, Y.; Luo, H. X.; Dai, L. M.; Qu, L. T. Vapor-Activated Power Generation on Conductive Polymer. *Adv. Funct. Mater.* **2016**, *26* (47), 8784−8792.
(42) Xu, T.; Ding, X.; Huang, Y.; Shao, C.; Song, L.; Gao, X.; Zhang, Z.; Qu, L. An efficient polymer moist-electric generator. *Energy Environ. Sci.* **2019**, *12* (3), 972−978.
(43) Huang, Y.; Cheng, H.; Shi, G.; Qu, L. Highly Efficient Moisture-Triggered Nanogenerator Based on Graphene Quantum Dots. *ACS Appl. Mater. Interfaces* **2017**, *9* (44), 38170−38175.
(44) Shao, C.; Gao, J.; Xu, T.; Ji, B.; Xiao, Y.; Gao, C.; Zhao, Y.; Qu, L. Wearable Fiberform hygroelectric generator. *Nano Energy* **2018**, *53*, 698−705.
(45) Chen, S.; Xia, H.; Ni, Q.-Q. A Wearable Sustainable Moisture-Induced Electricity Generator Based on rGO/GO/rGO Sandwich-Like Structural Film. *Adv. Electron. Mater.* **2021**, *7* (7), 2100222.
(46) Zhao, F.; Cheng, H.; Zhang, Z.; Jiang, L.; Qu, L. Direct Power Generation from a Graphene Oxide Film under Moisture. *Adv. Mater.* **2015**, *27* (29), 4351−4357.
(47) Huang, Y.; Cheng, H.; Yang, C.; Zhang, P.; Liao, Q.; Yao, H.; Shi, G.; Qu, L. Interface-mediated hygroelectric generator with an output voltage approaching 1.5 V. *Nat. Commun.* **2018**, *9* (1), 4166.
(48) Cheng, H.; Huang, Y.; Zhao, F.; Yang, C.; Zhang, P.; Jiang, L.; Shi, G.; Qu, L. Spontaneous power source in ambient air of a well-directionally reduced graphene oxide bulk. *Energy Environ. Sci.* **2018**, *11* (10), 2839−2845.
(49) Huang, Y.; Cheng, H.; Yang, C.; Yao, H.; Li, C.; Qu, L. All-region-applicable, continuous power supply of graphene oxide composite. *Energy Environ. Sci.* **2019**, *12* (6), 1848−1856.
(50) Zhao, F.; Liang, Y.; Cheng, H. H.; Jiang, L.; Qu, L. T. Highly efficient moisture-enabled electricity generation from graphene oxide frameworks. *Energy Environ. Sci.* **2016**, *9* (3), 912−916.
(51) Huang, Y.; Wang, C.; Shao, C.; Wang, B.; Chen, N.; Jin, H.; Cheng, H.; Qu, L. Graphene Oxide Assemblies for Sustainable Clean-Water Harvesting and Green-Electricity Generation. *Acc. Mater. Res.* **2021**, *2* (2), 97−107.
(52) Yu, W.; Sisi, L.; Haiyan, Y.; Jie, L. Progress in the functional modification of graphene/graphene oxide: a review. *RSC Adv.* **2020**, *10* (26), 15328−15345.
(53) Dikin, D. A.; Stankovich, S.; Zimney, E. J.; Piner, R. D.; Dommett, G. H. B.; Evmenenko, G.; Nguyen, S. T.; Ruoff, R. S. Preparation and characterization of graphene oxide paper. *Nature* **2007**, *448* (7152), 457−460.
(54) Liu, J.; Qi, Y.; Liu, D.; Dong, D.; Liu, D.; Li, Z. Moisture-enabled electricity generation from gradient polyoxometalates-modified sponge-like graphene oxide monolith. *J. Mater. Sci.* **2019**, *54* (6), 4831−4841.
(55) Xu, T.; Ding, X.; Shao, C.; Song, L.; Lin, T.; Gao, X.; Xue, J.; Zhang, Z.; Qu, L. Electric Power Generation through the Direct Interaction of Pristine Graphene-Oxide with Water Molecules. *Small* **2018**, *14* (14), 1704473.
(56) Yang, C.; Huang, Y.; Cheng, H.; Jiang, L.; Qu, L. Rollable, Stretchable, and Reconfigurable Graphene Hygroelectric Generators. *Adv. Mater.* **2019**, *31* (2), 1805705.
(57) Cheng, H.; Huang, Y.; Qu, L.; Cheng, Q.; Shi, G.; Jiang, L. Flexible in-plane graphene oxide moisture-electric converter for touchless interactive panel. *Nano Energy* **2018**, *45*, 37−43.
(58) Williams, P. M. Zeta Potential. In *Encyclopedia of Membranes*; Drioli, E., Giorno, L., Eds.; Springer: Berlin Heidelberg, Germany, 2016; pp 2063−2064.
(59) Ferraris, S.; Cazzola, M.; Peretti, V.; Stella, B.; Spriano, S. Zeta Potential Measurements on Solid Surfaces for in Vitro Biomaterials Testing: Surface Charge, Reactivity Upon Contact With Fluids and Protein Absorption. *Front. Bioeng. Biotechnol.* **2018**, *6* (60), 60.
(60) Liu, P.; Zhou, T.; Teng, Y.; Fu, L.; Hu, Y.; Lin, X.; Kong, X.-Y.; Jiang, L.; Wen, L. Light-Induced Heat Driving Active Ion Transport Based on 2D MXene Nanofluids for Enhancing Osmotic Energy Conversion. *CCS Chemistry* **2021**, *3* (4), 1325−1335.
(61) Zhang, H. C.; Li, X. Y.; Hou, J.; Jiang, L.; Wang, H. T. Angstrom-scale ion channels towards single-ion selectivity. *Chem. Soc. Rev.* **2022**, *51* (6), 2224−2254.
(62) Chen, G.; Sachar, H. S.; Das, S. Efficient electrochemomechanical energy conversion in nanochannels grafted with end-charged polyelectrolyte brushes at medium and high salt concentration. *Soft Matter* **2018**, *14* (25), 5246−5255.
(63) Loosli, F.; Le Coustumer, P.; Stoll, S. Impact of alginate concentration on the stability of agglomerates made of TiO_2 engineered nanoparticles: Water hardness and pH effects. *J. Nanopart. Res.* **2015**, *17*, 44.

https://doi.org/10.1021/acsanm.2c01557
ACS Appl. Nano Mater. XXXX, XXX, XXX−XXX

(64) Cooper, D. R.; D'Anjou, B.; Ghattamaneni, N.; Harack, B.; Hilke, M.; Horth, A.; Majlis, N.; Massicotte, M.; Vandsburger, L.; Whiteway, E.; et al. Experimental Review of Graphene. *ISRN Condens. Matter Phys.* **2012**, *2012*, 501686.
(65) Zhang, Z.; Li, X.; Yin, J.; Xu, Y.; Fei, W.; Xue, M.; Wang, Q.; Zhou, J.; Guo, W. Emerging hydrovoltaic technology. *Nat. Nanotechnol.* **2018**, *13* (12), 1109−1119.
(66) Ye, M.; Zhang, Z.; Zhao, Y.; Qu, L. Graphene Platforms for Smart Energy Generation and Storage. *Joule* **2018**, *2* (2), 245−268.
(67) Sahu, S.; Rout, G. C. Band gap opening in graphene: a short theoretical study. *Int. Nano Lett.* **2017**, *7* (2), 81−89.
(68) Suvarnaphaet, P.; Pechprasarn, S. Graphene-Based Materials for Biosensors: A Review. *Sensors* **2017**, *17* (10), 2161.
(69) Wang, D.; Chen, J.-F.; Dai, L. Recent Advances in Graphene Quantum Dots for Fluorescence Bioimaging from Cells through Tissues to Animals. *Part. Part. Syst. Charact.* **2015**, *32* (5), 515−523.
(70) Elvati, P.; Baumeister, E.; Violi, A. Graphene quantum dots: effect of size, composition and curvature on their assembly. *RSC Adv.* **2017**, *7* (29), 17704−17710.
(71) Zhao, C.; Song, X.; Liu, Y.; Fu, Y.; Ye, L.; Wang, N.; Wang, F.; Li, L.; Mohammadniaei, M.; Zhang, M.; et al. Synthesis of graphene quantum dots and their applications in drug delivery. *J. Nanobiotechnol.* **2020**, *18* (1), 142.
(72) Younis, M. R.; He, G.; Lin, J.; Huang, P. Recent Advances on Graphene Quantum Dots for Bioimaging Applications. *Front. Chem.* **2020**, *8*, 424.
(73) Biswas, C.; Lee, Y. H. Graphene Versus Carbon Nanotubes in Electronic Devices. *Adv. Funct. Mater.* **2011**, *21* (20), 3806−3826.
(74) Sinka, V.; Cruz, D. A.; López-Soria, J. M.; Martín, V. S.; Miranda, P. O.; Padrón, J. I. Synthesis of Heterocycles With Iron Salts as Sustainable Metal Catalysts. In *Advances in Transition-Metal Mediated Heterocyclic Synthesis*; Solé, D., Fernández, I., Eds.; Academic Press: London, 2018; pp 193−229.
(75) Liang, Y.; Zhao, F.; Cheng, Z.; Zhou, Q.; Shao, H.; Jiang, L.; Qu, L. Self-powered wearable graphene fiber for information expression. *Nano Energy* **2017**, *32*, 329−335.
(76) Liang, Y.; Wang, Z.; Huang, J.; Cheng, H.; Zhao, F.; Hu, Y.; Jiang, L.; Qu, L. Series of in-fiber graphene supercapacitors for flexible wearable devices. *J. Mater. Chem. A* **2015**, *3* (6), 2547−2551.
(77) Liang, Y.; Zhao, F.; Cheng, Z.; Deng, Y.; Xiao, Y.; Cheng, H.; Zhang, P.; Huang, Y.; Shao, H.; Qu, L. Electric power generation via asymmetric moisturizing of graphene oxide for flexible, printable and portable electronics. *Energy Environ. Sci.* **2018**, *11* (7), 1730−1735.
(78) Fan, K.; Liu, X.; Liu, Y.; Li, Y.; Liu, X.; Feng, W.; Wang, X. Spontaneous power generation from broad-humidity atmospheres through heterostructured F/O-bonded graphene monoliths. *Nano Energy* **2022**, *91*, 106605.
(79) Fan, Z.; Li, N.; Du, P.; Yang, W.; Chen, Q. Influence of Lattice Dynamics on the Proton Transport in BaZrY-Oxide Perovskites under High Pressure. *J. Phys. Chem. C* **2020**, *124* (41), 22376−22382.
(80) Fan, K.; Chen, X.; Wang, X.; Liu, X.; Liu, Y.; Lai, W.; Liu, X. Toward Excellent Tribological Performance as Oil-Based Lubricant Additive: Particular Tribological Behavior of Fluorinated Graphene. *ACS Appl. Mater. Interfaces* **2018**, *10* (34), 28828−28838.
(81) Nakamura, O.; Kodama, T.; Ogino, I.; Miyake, Y. High-Conductivity Solid Proton Conductors: Dodecamolybdophosphoric Acid and Dodecatungstophosphoric Acid Crystals. *Chem. Lett.* **1979**, *8* (1), 17−18.
(82) Zhu, R.; Zhu, Y.; Chen, F.; Patterson, R.; Zhou, Y.; Wan, T.; Hu, L.; Wu, T.; Joshi, R.; Li, M.; Cazorla, C.; Lu, Y.; Han, Z.; Chu, D. Boosting moisture induced electricity generation from graphene oxide through engineering oxygen-based functional groups. *Nano Energy* **2022**, *94*, 106942.
(83) Lommerse, J. P. M.; Price, S. L.; Taylor, R. Hydrogen bonding of carbonyl, ether, and ester oxygen atoms with alkanol hydroxyl groups. *J. Comput. Chem.* **1997**, *18* (6), 757−774.
(84) Yang, L.; Yang, F.; Liu, X.; Li, K.; Zhou, Y.; Wang, Y.; Yu, T.; Zhong, M.; Xu, X.; Zhang, L.; et al. A moisture-enabled fully printable power source inspired by electric eels. *Proc. Natl. Acad. Sci. U. S. A.* **2021**, *118* (16), e2023164118.
(85) Abraham, J.; Vasu, K. S.; Williams, C. D.; Gopinadhan, K.; Su, Y.; Cherian, C. T.; Dix, J.; Prestat, E.; Haigh, S. J.; Grigorieva, I. V.; Carbone, P.; Geim, A. K.; Nair, R. R. Tunable sieving of ions using graphene oxide membranes. *Nat. Nanotechnol.* **2017**, *12* (6), 546−550.
(86) Kim, S.; Zhou, S.; Hu, Y.; Acik, M.; Chabal, Y. J.; Berger, C.; de Heer, W.; Bongiorno, A.; Riedo, E. Room-temperature metastability of multilayer graphene oxide films. *Nat. Mater.* **2012**, *11* (6), 544−549.
(87) Luo, Z.; Liu, C.; Fan, S. A moisture induced self-charging device for energy harvesting and storage. *Nano Energy* **2019**, *60*, 371−376.
(88) Srinivasan, S.; Je, S. H.; Back, S.; Barin, G.; Buyukcakir, O.; Guliyev, R.; Jung, Y.; Coskun, A. Ordered Supramolecular Gels Based on Graphene Oxide and Tetracationic Cyclophanes. *Adv. Mater.* **2014**, *26* (17), 2725−2729.
(89) Ikeda, Y.; Karim, M. R.; Takehira, H.; Matsui, T.; Taniguchi, T.; Koinuma, M.; Matsumoto, Y.; Hayami, S. Proton Conductivity of Graphene Oxide Hybrids with Covalently Functionalized Alkylamines. *Chem. Lett.* **2013**, *42* (11), 1412−1414.
(90) Daripa, S.; Khawas, K.; Behere, R. P.; Verma, R.; Kuila, B. K. Efficient Moisture-Induced Energy Harvesting from Water-Soluble Conjugated Block Copolymer-Functionalized Reduced Graphene Oxide. *ACS Omega* **2021**, *6* (11), 7257−7265.
(91) Daripa, S.; Khawas, K.; Das, S.; Dey, R. K.; Kuila, B. K. Aligned Proton-Conducting Graphene Sheets via Block Copolymer Supramolecular Assembly and Their Application for Highly Transparent Moisture-Sensing Conductive Coating. *ChemistrySelect* **2019**, *4* (25), 7523−7531.
(92) Lv, D.; Zheng, S.; Cao, C.; Li, K.; Ai, L.; Li, X.; Yang, Z.; Xu, Z.; Yao, X. Defect-enhanced selective ion transport in an ionic nanocomposite for efficient energy harvesting from moisture. *Energy Environ. Sci.* **2022**, 2601−2609.
(93) Wang, H.; He, T.; Hao, X.; Huang, Y.; Yao, H.; Liu, F.; Cheng, H.; Qu, L. Moisture adsorption-desorption full cycle power generation. *Nat. Commun.* **2022**, *13* (1), 2524.
(94) Zhu, H. J.; Xu, Y. X.; Yan, Y. S.; Xu, J. B.; Yang, C. Interfacial Diffusion of Hydrated Ion on Graphene Surface: A Molecular Simulation Study. *Langmuir* **2020**, *36* (45), 13613−13620.
(95) Akhter, M. J.; Kus, W.; Mrozek, A.; Burczynski, T. Mechanical Properties of Monolayer MoS_2 with Randomly Distributed Defects. *Materials* **2020**, *13* (6), 1307.
(96) Tahir, M. B.; Fatima, U. Recent trends and emerging challenges in two-dimensional materials for energy harvesting and storage applications. *Energy Storage* **2022**, *4* (1), e244.
(97) Kuc, A.; Heine, T.; Kis, A. Electronic properties of transition-metal dichalcogenides. *MRS Bull.* **2015**, *40* (7), 577−584.
(98) Manzeli, S.; Ovchinnikov, D.; Pasquier, D.; Yazyev, O. V.; Kis, A. 2D transition metal dichalcogenides. *Nat. Rev. Mater.* **2017**, *2* (8), 17033.
(99) He, D.; Yang, Y.; Zhou, Y.; Wan, J.; Wang, H.; Fan, X.; Li, Q.; Huang, H. Electricity generation from phase-engineered flexible MoS_2 nanosheets under moisture. *Nano Energy* **2021**, *81*, 105630.
(100) Li, P.; Su, N.; Wang, Z.; Qiu, J. A Ti3C2Tx MXene-Based Energy-Harvesting Soft Actuator with Self-Powered Humidity Sensing and Real-Time Motion Tracking Capability. *ACS Nano* **2021**, *15* (10), 16811−16818.
(101) Wang, J.; Liu, Y.; Cheng, Z.; Xie, Z.; Yin, L.; Wang, W.; Song, Y.; Zhang, H.; Wang, Y.; Fan, Z. Highly Conductive MXene Film Actuator Based on Moisture Gradients. *Angew. Chem., Int. Ed.* **2020**, *59* (33), 14029−14033.
(102) Liu, J.; Zhang, H.-B.; Sun, R.; Liu, Y.; Liu, Z.; Zhou, A.; Yu, Z.-Z. Hydrophobic, Flexible, and Lightweight MXene Foams for High-Performance Electromagnetic-Interference Shielding. *Adv. Mater.* **2017**, *29* (38), 1702367.

https://doi.org/10.1021/acsanm.2c01557
ACS Appl. Nano Mater. XXXX, XXX, XXX−XXX

(103) Mehdi Aghaei, S.; Aasi, A.; Panchapakesan, B. Experimental and Theoretical Advances in MXene-Based Gas Sensors. *ACS Omega* **2021**, *6* (4), 2450−2461.
(104) Yang, L.; Cui, J.; Zhang, L.; Xu, X.; Chen, X.; Sun, D. A Moisture-Driven Actuator Based on Polydopamine-Modified MXene/Bacterial Cellulose Nanofiber Composite Film. *Adv. Funct. Mater.* **2021**, *31* (27), 2101378.
(105) Zhao, Q. N.; Jiang, Y. D.; Duan, Z. H.; Yuan, Z.; Zha, J. J.; Wu, Z. K.; Huang, Q.; Zhou, Z.; Li, H.; He, F.; Su, Y. J.; Tan, C. L.; Tai, H. L. A Nb_2CT_x/sodium alginate-based composite film with neuron-like network for self-powered humidity sensing. *Chem. Eng. J.* **2022**, *438*, 135588.
(106) Wang, Q. H.; Pan, X. F.; Wang, X. P.; Gao, H. L.; Chen, Y. B.; Chen, L.; Ni, Y. H.; Cao, S. L.; Ma, X. J. Spider web-inspired ultra-stable 3D $Ti_3C_2T_x$ (MXene) hydrogels constructed by temporary ultrasonic alignment and permanent in-situ self-assembly fixation. *Composites, Part B* **2020**, *197*, 108187.
(107) Yang, S.; Tao, X. M.; Chen, W.; Mao, J. F.; Luo, H.; Lin, S. P.; Zhang, L. S.; Hao, J. H. Ionic Hydrogel for Efficient and Scalable Moisture-Electric Generation. *Adv. Mater.* **2022**, *34*, 2200693.
(108) Ni, F.; Qiu, N. X.; Xiao, P.; Zhang, C.; Jian, Y. K.; Liang, Y.; Xie, W. P.; Yan, L. K.; Chen, T. Tillandsia-Inspired Hygroscopic Photothermal Organogels for Efficient Atmospheric Water Harvesting. *Angew. Chem., Int. Ed.* **2020**, *59* (43), 19237−19246.
(109) Wang, H. Y.; Cheng, H. H.; Huang, Y. X.; Yang, C.; Wang, D. B.; Li, C.; Qu, L. T. Transparent, self-healing, arbitrary tailorable moist-electric film generator. *Nano Energy* **2020**, *67*, 104238.
(110) Habel, J.; Ogbonna, A.; Larsen, N.; Cherré, S.; Kynde, S.; Midtgaard, S. R.; Kinoshita, K.; Krabbe, S.; Jensen, G. V.; Hansen, J. S.; Almdal, K.; Hèlix-Nielsen, C. Selecting analytical tools for characterization of polymersomes in aqueous solution. *RSC Adv.* **2015**, *5* (97), 79924−79946.
(111) Sun, Z.; Feng, L.; Xiong, C.; He, X.; Wang, L.; Qin, X.; Yu, J. Electrospun nanofiber fabric: an efficient, breathable and wearable moist-electric generator. *J. Mater. Chem. A* **2021**, *9* (11), 7085−7093.
(112) He, P.; Guo, R. S.; Hu, K.; Liu, K.; Lin, S.; Wu, H.; Huang, L. L.; Chen, L. H.; Ni, Y. H. Tough and super-stretchable conductive double network hydrogels with multiple sensations and moisture-electric generation. *Chem. Eng. J.* **2021**, *414*, 128726.
(113) Arndt, C.; Hauck, M.; Wacker, I.; Zeller-Plumhoff, B.; Rasch, F.; Taale, M.; Nia, A. S.; Feng, X. L.; Adelung, R.; Schroder, R. R.; Schutt, F.; Selhuber-Unkel, C. Microengineered Hollow Graphene Tube Systems Generate Conductive Hydrogels with Extremely Low Filler Concentration. *Nano Lett.* **2021**, *21* (8), 3690−3697.
(114) Yaghi, O. M.; O'Keeffe, M.; Ockwig, N. W.; Chae, H. K.; Eddaoudi, M.; Kim, J. Reticular synthesis and the design of new materials. *Nature* **2003**, *423* (6941), 705−714.
(115) Furukawa, H.; Cordova, K. E.; O'Keeffe, M.; Yaghi, O. M. The Chemistry and Applications of Metal-Organic Frameworks. *Science* **2013**, *341* (6149), 1230444.
(116) Bourrelly, S.; Llewellyn, P. L.; Serre, C.; Millange, F.; Loiseau, T.; Ferey, G. Different adsorption behaviors of methane and carbon dioxide in the isotypic nanoporous metal terephthalates MIL-53 and MIL-47. *J. Am. Chem. Soc.* **2005**, *127* (39), 13519−13521.
(117) Li, Y.; Yang, R. T. Gas adsorption and storage in metal-organic framework MOF-177. *Langmuir* **2007**, *23* (26), 12937−12944.
(118) Zhou, X. Y.; Lu, H. Y.; Zhao, F.; Yu, G. H. Atmospheric Water Harvesting: A Review of Material and Structural Designs. *ACS Mater. Lett.* **2020**, *2* (7), 671−684.
(119) Furukawa, H.; Gandara, F.; Zhang, Y. B.; Jiang, J. C.; Queen, W. L.; Hudson, M. R.; Yaghi, O. M. Water Adsorption in Porous Metal-Organic Frameworks and Related Materials. *J. Am. Chem. Soc.* **2014**, *136* (11), 4369−4381.
(120) Kim, H.; Yang, S.; Rao, S. R.; Narayanan, S.; Kapustin, E. A.; Furukawa, H.; Umans, A. S.; Yaghi, O. M.; Wang, E. N. Water harvesting from air with metal-organic frameworks powered by natural sunlight. *Science* **2017**, *356* (6336), 430−432.
(121) Fathieh, F.; Kalmutzki, M. J.; Kapustin, E. A.; Waller, P. J.; Yang, J. J.; Yaghi, O. M. Practical water production from desert air. *Sci. Adv.* **2018**, *4* (6), eaat3198.
(122) Yang, W. Q.; Li, X. K.; Han, X.; Zhang, W. H.; Wang, Z. B.; Ma, X. M.; Li, M. J.; Li, C. X. Asymmetric ionic aerogel of biologic nanofibrils for harvesting electricity from moisture. *Nano Energy* **2020**, *71*, 104610.
(123) Gao, X.; Xu, T.; Shao, C.; Han, Y.; Lu, B.; Zhang, Z.; Qu, L. Electric power generation using paper materials. *J. Mater. Chem. A* **2019**, *7* (36), 20574−20578.
(124) Li, M. J.; Zong, L.; Yang, W. Q.; Li, X. K.; You, J.; Wu, X. C.; Li, Z. H.; Li, C. X. Biological Nanofibrous Generator for Electricity Harvest from Moist Air Flow. *Adv. Funct. Mater.* **2019**, *29*, 1901798.
(125) Han, X.; Zhang, W. H.; Che, X. P.; Long, L. F.; Li, M. J.; Li, C. X. Synergetic and persistent harvesting of electricity and potable water from ambient moisture with biohybrid fibrils. *J. Mater. Chem. A* **2022**, *10* (15), 8356−8363.
(126) Rauf, S.; Vijjapu, M. T.; Andres, M. A.; Gascon, I.; Roubeau, O.; Eddaoudi, M.; Salama, K. N. Highly Selective Metal-Organic Framework Textile Humidity Sensor. *ACS Appl. Mater. Interfaces* **2020**, *12* (26), 29999−30006.
(127) Andres, M. A.; Vijjapu, M. T.; Surya, S. G.; Shekhah, O.; Salama, K. N.; Serre, C.; Eddaoudi, M.; Roubeau, O.; Gascon, I. Methanol and Humidity Capacitive Sensors Based on Thin Films of MOF Nanoparticles. *ACS Appl. Mater. Interfaces* **2020**, *12* (3), 4155−4162.
(128) Weiss, A.; Reimer, N.; Stock, N.; Tiemann, M.; Wagner, T. Surface-modified CAU-10 MOF materials as humidity sensors: impedance spectroscopic study on water uptake. *Phys. Chem. Chem. Phys.* **2015**, *17* (33), 21634−21642.
(129) Benoit, V.; Chanut, N.; Pillai, R. S.; Benzaqui, M.; Beurroies, I.; Devautour-Vinot, S.; Serre, C.; Steunou, N.; Maurin, G.; Llewellyn, P. L. A promising metal-organic framework (MOF), MIL-96(Al), for CO2 separation under humid conditions. *J. Mater. Chem. A* **2018**, *6* (5), 2081−2090.
(130) Reinsch, H.; van der Veen, M. A.; Gil, B.; Marszalek, B.; Verbiest, T.; de Vos, D.; Stock, N. Structures, Sorption Characteristics, and Nonlinear Optical Properties of a New Series of Highly Stable Aluminum MOFs. *Chem. Mater.* **2013**, *25* (1), 17−26.
(131) Kusgens, P.; Rose, M.; Senkovska, I.; Frode, H.; Henschel, A.; Siegle, S.; Kaskel, S. Characterization of metal-organic frameworks by water adsorption. *Microporous Mesoporous Mater.* **2009**, *120* (3), 325−330.
(132) Kwak, S. S.; Lin, S. S.; Lee, J. H.; Ryu, H.; Kim, T. Y.; Zhong, H. K.; Chen, H. S.; Kim, S. W. Triboelectrification-Induced Large Electric Power Generation from a Single Moving Droplet on Graphene/Polytetrafluoroethylene. *ACS Nano* **2016**, *10* (8), 7297−7302.
(133) Zhong, H. K.; Wu, Z. Q.; Li, X. Q.; Xu, W. L.; Xu, S.; Zhang, S. J.; Xu, Z. J.; Chen, H. S.; Lin, S. S. Graphene based two dimensional hybrid nanogenerator for concurrently harvesting energy from sunlight and water flow. *Carbon* **2016**, *105*, 199−204.
(134) Dhiman, P.; Yavari, F.; Mi, X.; Gullapalli, H.; Shi, Y. F.; Ajayan, P. M.; Koratkar, N. Harvesting Energy from Water Flow over Graphene. *Nano Lett.* **2011**, *11* (8), 3123−3127.
(135) Shen, D.; Xiao, M.; Zou, G.; Liu, L.; Duley, W. W.; Zhou, Y. N. Self-Powered Wearable Electronics Based on Moisture Enabled Electricity Generation. *Adv. Mater.* **2018**, *30*, 1705925.
(136) Crimp, M. J.; Oppermann, D. A.; Krehbiel, K. Suspension properties of hexagonal BN powders: effect of pH and oxygen content. *J. Mater. Sci.* **1999**, *34* (11), 2621−2625.
(137) Joni, I. M.; Balgis, R.; Ogi, T.; Iwaki, T.; Okuyama, K. Surface functionalization for dispersing and stabilizing hexagonal boron nitride nanoparticle by bead milling. *Colloid Surface A* **2011**, *388* (1−3), 49−58.
(138) Cao, X. B.; Qi, D. P.; Yin, S. Y.; Bu, J.; Li, F. J.; Goh, C. F.; Zhang, S.; Chen, X. D. Ambient Fabrication of Large-Area Graphene Films via a Synchronous Reduction and Assembly Strategy. *Adv. Mater.* **2013**, *25* (21), 2957−2962.

https://doi.org/10.1021/acsanm.2c01557
ACS Appl. Nano Mater. XXXX, XXX, XXX−XXX

(139) Ji, X.; Ying, Y.; Ge, C.; Zhu, Y.; Wang, K.; Di, Y.; Wang, S.; Li, D.; Zhang, J.; Hu, P.; Qiu, Y. Asymmetrically synchronous reduction and assembly of graphene oxide film on metal foil for moisture responsive actuator. *Nanotechnology* **2019**, *30* (44), 445601.
(140) Zhang, B.; Wang, K.; Ji, X.; Wang, S.; ma, Z.; Qiu, Y. A self-powered moisture detector using graphene oxide film constructed by asymmetric metal electrodes. *J. Alloys Compd.* **2019**, *810*, 151880.
(141) Hu, K.; Xiong, R.; Guo, H.; Ma, R.; Zhang, S.; Wang, Z. L.; Tsukruk, V. V. Self-Powered Electronic Skin with Biotactile Selectivity. *Adv. Mater.* **2016**, *28* (18), 3549−3556.
(142) Hu, K. S.; Tolentino, L. S.; Kulkarni, D. D.; Ye, C. H.; Kumar, S.; Tsukruk, V. V. Written-in Conductive Patterns on Robust Graphene Oxide Biopaper by Electrochemical Microstamping. *Angew. Chem., Int. Ed.* **2013**, *52* (51), 13784−13788.
(143) Sun, Z. Y.; Feng, L. L.; Wen, X.; Wang, L. M.; Qin, X. H.; Yu, J. Y. Nanofiber fabric based ion-gradient-enhanced moist-electric generator with a sustained voltage output of 1.1 V. *Mater. Horiz.* **2021**, *8* (8), 2303−2309.
(144) Huang, L.; Xu, S.; Wang, Z.; Xue, K.; Su, J.; Song, Y.; Chen, S.; Zhu, C.; Tang, B. Z.; Ye, R. Self-Reporting and Photothermally Enhanced Rapid Bacterial Killing on a Laser-Induced Graphene Mask. *ACS Nano* **2020**, *14* (9), 12045−12053.
(145) Xu, Y.; Fei, Q.; Page, M.; Zhao, G.; Ling, Y.; Chen, D.; Yan, Z. Laser-induced graphene for bioelectronics and soft actuators. *Nano Res.* **2021**, *14* (9), 3033−3050.
(146) Lee, S.; Jang, H.; Lee, H.; Yoon, D.; Jeon, S. Direct Fabrication of a Moisture-Driven Power Generator by Laser-Induced Graphitization with a Gradual Defocusing Method. *ACS Appl. Mater. Interfaces* **2019**, *11* (30), 26970−26975.
(147) Wang, Z.; Shen, Q.; Zhang, J.; Jiang, M.; Chen, W.; Tao, P.; Song, C.; Fu, B.; Deng, T.; Shang, W. Self-powered infrared detection using a graphene oxide film. *J. Mater. Chem. A* **2020**, *8* (18), 9248−9255.
(148) Han, Y. Y.; Lu, B.; Shao, C. X.; Xu, T.; Liu, Q. W.; Liang, Y.; Jin, X. T.; Gao, J.; Zhang, Z. P. A hygroelectric power generator with energy self-storage. *Chem. Eng. J.* **2020**, *384*, 123366.
(149) Zhao, F.; Wang, L.; Zhao, Y.; Qu, L.; Dai, L. Graphene Oxide Nanoribbon Assembly toward Moisture-Powered Information Storage. *Adv. Mater.* **2017**, *29* (3), 1604972.
(150) Tao, Y.; Wang, Z.; Xu, H.; Ding, W.; Zhao, X.; Lin, Y.; Liu, Y. Moisture-powered memristor with interfacial oxygen migration for power-free reading of multiple memory states. *Nano Energy* **2020**, *71*, 104628.
(151) Shen, D.; Xiao, Y.; Zou, G.; Liu, L.; Wu, A.; Xiao, M.; Feng, J.; Hui, Z.; Duley, W. W.; Zhou, Y. N. Exhaling-Driven Hydroelectric Nanogenerators for Stand-Alone Nonmechanical Breath Analyzing. *Adv. Mater. Technol.* **2020**, *5* (1), 1900819.
(152) Wang, Y.; Dai, M.; Wu, H.; Xu, L.; Zhang, T.; Chen, W.; Wang, Z. L.; Yang, Y. Moisture induced electricity for self-powered microrobots. *Nano Energy* **2021**, *90*, 106499.

https://doi.org/10.1021/acsanm.2c01557
ACS Appl. Nano Mater. XXXX, XXX, XXX−XXX